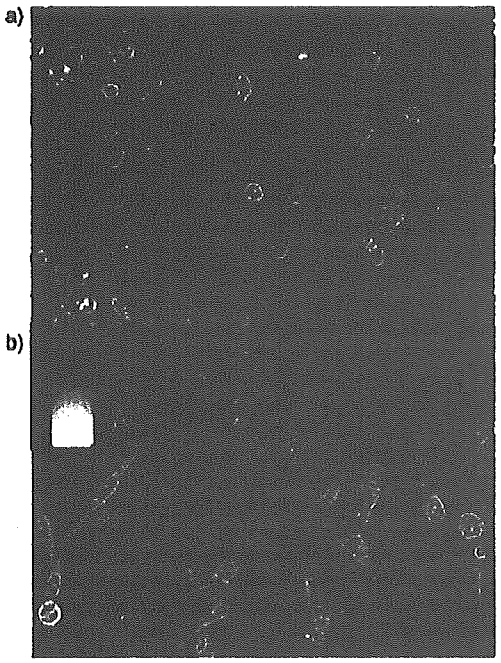

Figure 6. Overlay of the transmission and fluorescence microscope images of a) HeLa cells in the absence of any quantum dots and b) HeLa cells with silicon quantum dots incorporated inside the cytosol. Inset: fluorescence from a vial of allylamine-capped silicon quantum dots in water when excited with a UV lamp.

cence imaging. This result has major implications towards using colloidal silicon quantum dots effectively in biological fluorescence imaging.

In summary, silicon quantum dots with a narrow size distribution were synthesized using reverse micelles and powerful hydride reducing agents at room temperature and pressure. The surface of the silicon quantum dots was made hydrophilic by modification with allylamine. The silicon quantum dots dispersed in an aqueous environment displayed strong photoluminescence in the blue region of the visible spectrum, with a 10% quantum yield for the photoluminescence. The optical properties of the silicon quantum dots displayed features in both the absorption and emission spectra attributed to the direct band gap transitions in silicon quantum dots with a carbon surface termination. Time-resolved photoluminescence spectroscopy revealed a rapid recombination normally associated with direct band gap materials. The ease of synthesis and optical properties make the silicon quantum dots reported here excellent candidates for biomedical applications, as demonstrated by the imaging of allylamine-capped silicon quantum dots in HeLa cells.

Experimental Section

Synthesis of allylamine-capped silicon quantum dots: Silicon quantum dots were synthesized in reverse micelles by the solution-phase reduction of $SiCl_4$ with 1 M $LiAlH_4$ in THF (Aldrich). The surfactant and solvent combination used to form the micelles were tetraoctylammonium bromide (TOAB, Merck) in toluene. Surface modification of the silicon quantum dots was achieved by treating the surface of the particles with allylamine (Aldrich). All experiments were carried out in an argon atmosphere in a glove box to prevent oxidation of the silicon. Oxygen levels were below 10 ppm at all times.

In a typical experiment, $SiCl_4$ (92 μL, 0.0008 mol) was dissolved in TOAB (1.5 g) and anhydrous toluene (100 mL) by using a homogenizer. Silicon quantum dots were then formed by adding a twofold excess of reducing agent. The mixture was left to react for 3 h and then anhydrous methanol (20 mL) was slowly added to quench any excess reducing agent. At this point it is expected that the surface of the particles were terminated with hydrogen.[20,25] Hydrophilic particles were formed by modifying the surface silicon–hydrogen bonds by reaction with 0.05 M H_2PtCl_6 (40 μL) in isopropanol as the catalyst and allylamine (2 mL). After modification of the surface, the sample was removed from the glove box and purified by removing the surfactant.[32] The solvent was then removed using a rotary evaporator to produce a white powder consisting of mainly TOAB and silicon quantum dots. Distilled water (50 mL) was then added to the flask and resulted in the hydrophilic silicon quantum dots dissolving, but not the TOAB. The TOAB was then removed by successive filtration through a 0.22-μm membrane filter.

Incorporation of silicon quantum dots into HeLa cells: The HeLa cells were cultured in DMEM/F12 supplemented with 10% heat-inactivated fetal bovine serum at 37°C. The cells were plated at a volume of 1×10^6 cells/well on a 6-well culture plate (Iwaki technoglass, Japan) and were stimulated with a solution of 0.2 nM Si quantum dots. After incubation of the mixtures for 12 h, the cells were washed with a phosphate-buffered saline (PBS) twice to remove the nonspecific binding quantum dots. The cells were then fixed with 1% paraformaldehyde in PBS for 5 min.[33] Fluorescence images of the HeLa cells were acquired with a digital camera D1X (Nikon) on a fluorescent microscope IX-81 (Olympus) using a mirror unit to adjust the excitation wavelength to 365 nm and an oil immersion objective lens. The blue fluorescent light was detected in the cytosol of each cell.

Received: April 11, 2005
Published online: ■■ ■■, ■■■■

Keywords: imaging agents · luminescence · nanostructures · quantum dots · silicon

[1] W. C. Chan, S. Nie, *Science* **1998**, *281*, 2016.
[2] M. Bruchez, M. Moronne, P. Gin, S. Weiss, A. P. Alivisatos, *Science* **1998**, *281*, 2013.
[3] M. Green, *Angew. Chem.* **2004**, *116*, 4221; *Angew. Chem. Int. Ed.* **2004**, *43*, 4129.
[4] A. Wu, H. Liu, J. Liu, K. N. Haley, J. A. Tradway, J. P. Larson, N. Ge, F. Peale, M. P. Bruchez, *Nat. Biotechnol.* **2003**, *21*, 41.
[5] B. Dubertret, P. Skourides, D. J. Norris, V. Noireaux, A. H. Brivanlou, A. Libchaber, *Science* **2002**, *298*, 1759.
[6] D. R. Larson, W. R. Zipfel, R. M. Williams, S. W. Clark, M. P. Bruchez, F. W. Wise, W. W. Webb, *Science* **2003**, *300*, 1434.
[7] L. Bakueva, G. Konstantatos, L. Levina, S. Musikhin, E. H. Sargent, *Appl. Phys. Lett.* **2004**, *84*, 3459.
[8] S. A. McDonald, P. W. Cyr, L. Levina, E. H. Sargent, *Appl. Phys. Lett.* **2004**, *85*, 2089.
[9] S. Coe, W. Woo, M. Bawendi, V. Bulovic, *Nature* **2002**, *420*, 800.
[10] T. Tsutsui, *Nature* **2002**, *420*, 752.
[11] W. U. Huynh, J. J. Dittmer, A. P. Alivisatos, *Science* **2002**, *295*, 2425.
[12] R. A. M. Hikmet, D. V. Talapin, H. Weller, *J. Appl. Phys.* **2003**, *93*, 3509.
[13] B. Sun, E. Marx, N. C. Greenham, *Nano Lett.* **2003**, *3*, 961.
[14] C. B. Murray, D. J. Norris, M. G. Bawendi, *J. Am. Chem. Soc.* **1993**, *115*, 8706.

[15] A. M. Derfus, W. C. W. Chan, S. N. Bhatia, *Nano Lett.* **2004**, *4*, 11.
[16] D. K. Nagesha, M. A. Whitehead, J. L. Coffer, *Adv. Mater.* **2005**, *17*, 921.
[17] L. T. Canham, C. L. Reeves, J. P. Newey, M. R. Houlton, T. I. Cox, J. M. Buriak, M. P. Stewart, *Adv. Mater.* **1999**, *11*, 1505.
[18] Z. Zhou, L. Brus, R. Friesner, *Nano Lett.* **2003**, *3*, 163.
[19] J. D. Holmes, K. J. Ziegler, C. Doty, L. E. Pell, K. P. Johnson, B. A. Korgel, *J. Am. Chem. Soc.* **2001**, *123*, 3748.
[20] J. P. Wilcoxon, P. P. Provencio, G. A. Samara, *Phys. Rev. B* **1999**, *60*, 2704.
[21] R. K. Baldwin, K. A. Pettigrew, E. Ratai, M. P. Augustine, S. M. Kauzlarich, *Chem. Commun.* **2002**, 1822.
[22] J. Zou, R. K. Baldwin, K. A. Pettigrew, S. M. Kauzlarich, *Nano Lett.* **2004**, *4*, 1181.
[23] D. S. English, L. E. Pell, Z. Yu, P. F. Barbara, B. A. Korgel, *Nano Lett.* **2002**, *2*, 681.
[24] J. P. Wilcoxon, G. A. Samara, *Appl. Phys. Lett.* **1999**, *74*, 3164.
[25] R. D. Tilley, J. H. Warner, K. Yamamoto, I. Matsui, H. Fujimori, *Chem. Commun.* **2005**, *14*, 1836.
[26] A. Puzder, A. J. Williamson, J. C. Grossman, G. Galli, *J. Am. Chem. Soc.* **2003**, *125*, 2786.
[27] C. Yang, R. A. Bley, S. M. Kauzlarich, H. W. H. Lee, G. R. Delgado, *J. Am. Chem. Soc.* **1999**, *121*, 5191.
[28] A. T. R. Williams, S. A. Winfield, J. N. Miller, *Analyst* **1983**, *108*, 1067.
[29] S. Hamai, F. Hirayama, *J. Phys. Chem.* **1983**, *87*, 83.
[30] Y. Kanemitsu, T. Futagi, T. Matsumoto, H. Mimura, *Phys. Rev. B* **1994**, *49*, 14732.
[31] J. H. Warner, E. Thomsen, A. R. Watt, N. R. Heckenberg, H. Rubinsztein-Dunlop, *Nanotechnology* **2005**, *16*, 175.
[32] R. D. Tilley, S. Saito, *Langmuir* **2003**, *19*, 5115.
[33] A. Hoshino, K. Fujioka, T. Oku, M. Suga, Y. F. Sasaki, T. Ohta, M. Yasuhara, K. Suzuki, K. Yamamoto, *Nano Lett.* **2004**, *4*, 2163.

Condensation Reactions of Amino Acids under Hydrothermal Conditions with Adiabatic Expansion Cooling

Tomomasa GOTO[1], Yasuhiro FUTAMURA[2,3], Yukio YAMAGUCHI[1] and Kenji YAMAMOTO[1,2]

[1]*Department of Chemical System Engineering, Graduate School of Engineering, The University of Tokyo, 3-1, Hongo 7, Bunkyou-ku, Tokyo 113-8656, Japan*

[2]*Department of Medical Ecology and Informatics, Research Institute, International Medical Center of Japan, 21-1, Toyama 1, Shinjuku-ku, Tokyo 162-8655, Japan*

[3]*Department of Bioactive Molecules, The National Institute of Infectious Diseases, 23-1, Toyama 1, Shinjuku-ku, Tokyo 162-8640, Japan*

Keywords: Peptide Polymerization, Adiabatic Expansion, Hydrothermal System, Prevention from Hydrolysis Reaction, Origin of Life

A novel flow reactor adopted for the adiabatic expansion cooling method, a rapid quenching method, was designed to synthesize oligopeptides from amino acids under hydrothermal conditions. We studied the hydrothermal reaction under the two experimental conditions, whose raw materials were glycine and diglycine aqueous solution. The temperature, the pressure and the residence time of the reaction were 270°C, 10 MPa and 27 seconds, respectively. Then we could obtain long oligoglycines like octa-, nona- and decaglycine. The concentration profiles of each product in the two experimental conditions were similar. It suggests that the equilibrium relations would be established between condensation reactions and hydrolysis reactions of oligoglycines, which might light up a new pathway to the study of the origin of life.

Introduction

We designed a novel flow reactor for synthesizing oligopeptides from amino acids in subcritical and supercritical water. In this reactor the method for quenching the solution after the reaction was adopted for the adiabatic expansion. We hypothesized that the method for quenching the solution had to be so rapid that we could obtain long oligopeptides. Shock (1992) reported that the thermodynamic equilibrium would shift to the condensation of amino acids as the temperature increased. This report suggests that the rapid quenching, a non-equilibrium method, could avoid hydrolysis and dissociation of the oligopeptides, which had already been synthesized under hydrothermal conditions. In short, the rapid quenching method such as the adiabatic expansion made it feasible that the oligopeptides were brought into our hands at room temperature and the atmospheric pressure. Here, the abundance ratio of products was kept at the equilibrium between condensation and hydrolysis of oligopeptides at high temperature and high pressure.

Several studies suggest the importance of quenching speed (Imai *et al.*, 1999; Ogata *et al.*, 2000; Alargov *et al.*, 2002; Islam *et al.*, 2003). In the study of Ogata *et al.* (2000) the method for cooling after the reaction that had been already heated at 250°C and pressurized at 24 MPa, was to pour the solution into a cold water bath whose pressure was somewhat higher than the atmospheric pressure. They found that di-, tri- and hexaglycine were synthesized from glycine without adding metal ions. Both Islam *et al.* (2003) and Alargov *et al.* (2002) applied another method to quenching the solution. After the glycine aqueous solution reacted at high temperature and high pressure, it passed through a cooling tube, the outside of which was bathed in cold water. However, the two research groups failed in synthesizing longer peptides like hexaglycine although their reaction conditions, the temperature and the pressure, were similar to those in the study of Ogata *et al.* (2000). The quenching method was supposed to play a key role in making their results differ greatly from each other. In fact, the method of pouring the solution into

Received on November 11, 2004. Correspondence concerning this article should be addressed to K. Yamamoto (E-mail address: backen@ri.imcj.go.jp).

Partly presented at the 36th Autumn Meeting of the Society of Chemical Engineers, Japan, at Sendai, September 2003, at the 10th Asian Pacific Confederation of Chemical Engineering, Japan, at Kitakyushu, October 2004, and at the 70th Annual Meeting of the Society of Chemical Engineers, Japan, at Nagoya, March 2005.

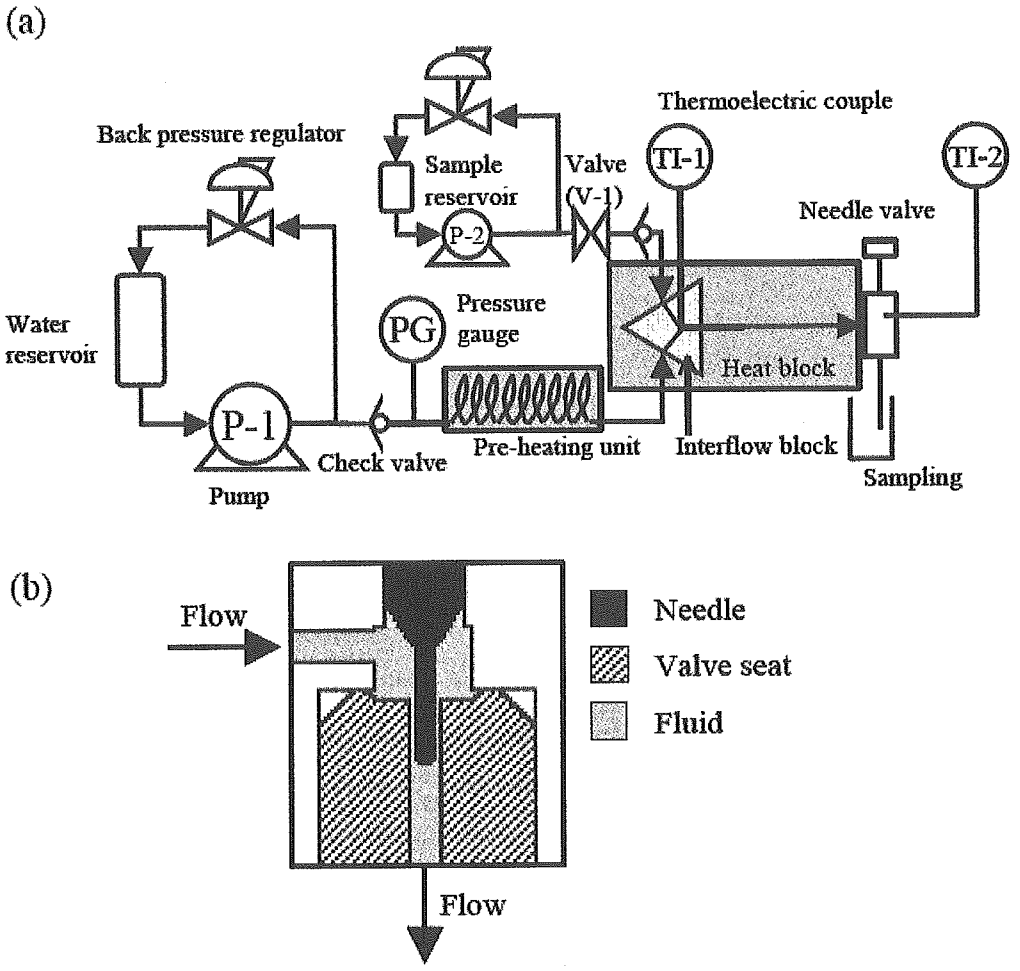

Fig. 1 (a) The experimental apparatus adopted for the adiabatic expansion cooling with a needle valve to reduce the hydrolysis reaction of the products; This flow reactor was designed to endure up to 40 MPa and 500°C. Almost all the parts that contacted with the solution were made of stainless steel SUS316. A stainless tube, by which a heat block kept heated, was placed between an interflow block and an inlet of a needle valve. The volume of the tube was 1.5 mL. (b) The detailed view inside the needle valve; the needle was attached to a valve seat and there was a very small gap between the needle and the valve seat. The pressure of the reactor was controlled with two back pressure regulators and the needle valve

the cold bath more rapidly resulted in the synthesis of the longer oligoglycine.

The adiabatic expansion cooling was thought to be one of the most rapid methods for quenching the solution. When the solution that had reacted at high temperature and high pressure was erupted into the atmosphere through the needle valve, it was both depressurized and cooled quickly with the Joule-Thomson effect. We used this method to reduce the decomposition of products. In this paper we demonstrated that the adiabatic expansion cooling method was an appropriate one to obtain the longer peptide and the equilibrium relation between condensation and hydrolysis of oligoglycines under hydrothermal conditions would be established.

1. Experimental

The flow diagram of the experimental apparatus we designed is shown in **Figure 1(a)**. This flow reactor was designed to endure high pressure and high temperature, up to 40 MPa and 500°C respectively. Almost all the parts that contacted with solution were made of stainless steel SUS316. The apparatus had two reservoirs, one was for water and the other was for the sample solution. Water was pressurized by the pump P-1 (NP-KX-500-20; Nihon Seimitsu Kagaku Co., Ltd.) and was heated with the pre-heating unit. On the other hand, the pump P-2 (NP-D-324; Nihon Seimitsu Kagaku Co., Ltd.) pressurized the sample solution. In order to raise the temperature of the sample solution rapidly, the sample solution and heated water were mixed together in the interflow block whose temperature was monitored with a thermoelectric couple

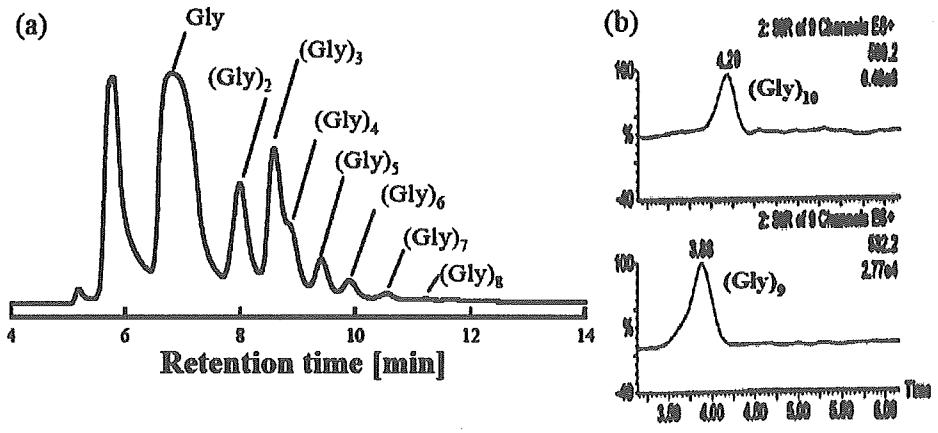

Fig. 2 (a) An high performance liquid chromatography (HPLC) profile of the products in the sample that reacted from 1.0 M glycine aqueous solution at 270°C and 10 MPa. (b) Selected Ion Monitoring (SIM) chromatograms of decaglycine (top) and nonaglycine (bottom); $(Gly)_i$ denotes the i-mer of glycine. The profile and the chromatograms were obtained from the HPLC system and the LC/MS system respectively, with the use of the same reverse-phased column (Waters Xterra MS C_{18} 2.5 mm; 4.6 × 50 mm). An aqueous solution of 50 mM KH_2PO_4 within 7.2 mM $C_6H_{13}SO_3Na$ (pH = 2.5) was used as a mobile phase in the condition for (a). The UV detector monitored the absorbance at 200 nm. In the condition for (b), an aqueous solution of 1 mM $C_5F_{11}COOH$ was used as a mobile phase and the oligoglycines were detected in the Selected Ion Recording (SIR) mode

(TD-11S; SHIMADEN Co., Ltd.). A stainless tube, by which the heat block kept heated, was placed between the interflow block and the inlet of a needle valve. The volume of the tube where material would react was 1.5 mL. Figure 1(**b**) is the details of the inside of the needle valve. The needle was connected with the valve seat and there was a very small gap between the needle and the valve seat. The pressure of the reactor was controlled with two back pressure regulators and the needle valve. To keep the solution heated just before adiabatic expansion cooling, the needle valve was also kept heated. The needle valve made it feasible that the solution was quenched more rapidly than by a water-cooling unit, a conventional method. Therefore it was expected that hydrolysis or decomposition of the products would be suppressed during quenching and depressurizing the solution.

We analyzed the products in an aqueous solution with a high performance liquid chromatography, HPLC, (600E Multisolvent Delivery System and 2487 Dual λ absorbance Detector; Waters Co.) to identify and quantify oligoglycines. A reverse-phased column (Waters Xterra MS C_{18} 2.5 mm; 4.6 × 50 mm) was applied and an aqueous solution of 50 mM KH_2PO_4 within 7.2 mM $C_6H_{13}SO_3Na$ (pH = 2.5) was used as a mobile phase (Tucker *et al.*, 1989). The flow rate of the mobile phase was 0.5 mL/min and the UV detector monitored the absorbance at 200 nm. We also used a Liquid chromatography/Mass spectrometer system, LC/MS, (2695 separation module and Micromass ZQ2000 mass spectrometer; Waters Co.) in order to identify too long oligoglycines to be available as a standard, like nonaglycine and decaglycine. The column was the reverse-phased column as described above and the mobile phase was an aqueous solution of 1 mM $C_5F_{11}COOH$ (Pearson and McCroskey, 1996). Oligoglycines were detected in the Selected Ion Recording mode.

Glycine, glycine anhydride and 1-hexane sulfonic acid sodium salt were purchased from Wako Pure Chemical Industries, Ltd. Diglycine, triglycine, tetraglycine, pentaglycine, hexaglycine, Phosphoric acid and Potassium dihydrogen phosphate were purchased from Sigma-Aldrich Co. Heptaglycine and octaglycine were purchased from Invitrogen Co. The purified water was from Kozakai Seiyaku Co., Ltd. Undecafluorohexaonic acid was purchased from Tokyo Kasei Kogyo Co., Ltd.

2. Results and Discussion

Water was heated to nearly 500°C in the pre-heating unit and was pressurized at 10 MPa by the pump P-1 whose flow rate was 1.3 mL/min. At the same time, sample solutions, 2.0 M glycine and 1.5 M diglycine aqueous solutions, were put into the sample reservoir and was pressurized by the pump P-2 whose rate was also 1.3 mL/min because the concentration of the glycine and diglycine solution after the mixing in the interflow block would be 1.0 M and 0.75 M respectively. Considering the density of water at 270°C and 10 MPa, the residence time of the reaction was always 27 seconds. With the rate of the input being 2.6 mL/min, the needle valve was controlled so that its rate of the output would be about 2.6 mL/min. Moreover, both the heat block and the needle valve were heated to the

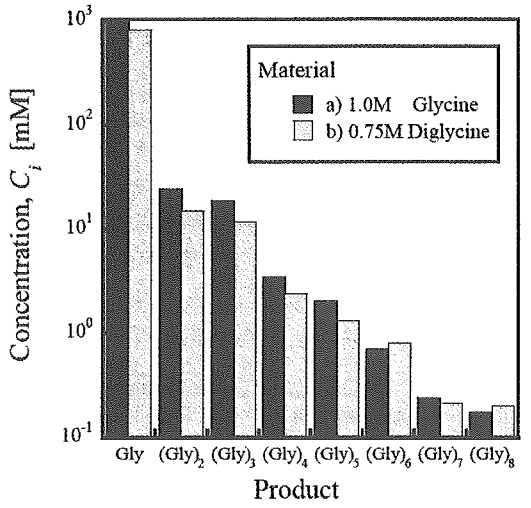

Fig. 3 The concentration profiles of the products in the two samples that obtained from (a) 1.0 M glycine and (b) 0.75 M diglycine aqueous solutions at 270°C and 10 MPa without the compensation by the concentration in erupting and expanding; $(Gly)_i$ denotes the i-mer of glycine

reaction temperature of 270°C. After the reaction in highly heated and highly pressurized water, the solution was rapidly quenched and depressurized by the needle valve.

We have sampled reaction solutions at the outlet of the needle valve in two kinds of experiments whose raw material was 1.0 M glycine and 0.75 M diglycine aqueous solution respectively. The samples had been already concentrated about three times because of erupting and expanding to the open system. We analyzed the two samples with the HPLC system to identify and quantify their products. **Figure 2(a)** shows an HPLC profile of the products in the solution that obtained from 1.0 M glycine aqueous solution at 270°C and 10 MPa, which resulted in identifying the products with glycine, di-, tri-, tetra-, penta-, hexa-, hepta- and octaglycine. The peak at five minutes was the void peak of the HPLC system and the peak around six minutes mainly came from glycine anhydride including unknown products. The products of the other sample that obtained from 0.75 M diglycine were also confirmed with an HPLC profile (Data not shown). What is more, we have detected a certain amount of nonaglycine and decaglycine with the LC/MS system (Figure 2(**b**)). We have not confirmed whether undecaglycine or longer oligoglycines were produced or not. However, it is suggested that the adiabatic expansion cooling method was an effective way to obtain oligopeptides.

Figure 3 shows the concentration profiles of the products starting from glycine or diglycine. The value of concentration C_i, where i is the degree of condensation, in the two profiles wasn't considered with the compensation by the concentration when the solution was erupting and expanding to the open system. The higher the value of i, the degree of condensation of the product, was, the lower the value of C_i, the concentrations of oligoglycines, were. The profiles were so similar that we could consider that the residence time of the reaction, 27 seconds, had been sufficient to finish the two reactions, condensation and hydrolysis. It could be predicted that under hydrothermal conditions the equilibrium relations would be established between the condensation reaction and the hydrolysis reaction of oligoglycines.

Here, we calculated the rate of the loss of glycine (L) with the process as follows:

$$L = \frac{\left(C_0 - \sum iC_i^*\right)}{C_0}$$

where C_0 is defined as the concentration of material (glycine 1.0 M or diglycine 0.75 M) and C_i^* is defined as the compensated C_i by evaporation. We got the values of the loss of glycine obtained under the conditions (a) and (b) as 67 % and 68 % respectively, where the peak around six minutes in Figure 2(a) was supposed to be just composed of glycine anhydride. This indicated that more than a half of the material did not react into oligoglycine. It was possible that the material was decomposed into such compounds as ammonia, carbon dioxide and organic acids, which was inferred from Sato's study (Sato *et al.*, 2002). However we didn't analyze the side reaction.

In this paper, we demonstrated that the adiabatic expansion cooling method was one of the most proper processes of quenching the solution to polymerize peptides from amino acid. It might be thought that the adiabatic expansion cooling method made it feasible to obtain peptide easily with keeping the equilibrium stage between condensation and hydrolysis of oligopeptides at high temperature and high pressure. The hydrothermal reactor with the adiabatic expansion was so effective in polymerizing the amino acid that we could synthesize oligoglycine from glycine monomers, which could light up a new pathway not only in the field of chemical engineering but also in the study of the origin of life.

Acknowledgment

This work is partly supported by the research grant for "Learning from Nature for Production" from Sekisui Chemical Co., Ltd. and by the Ministry of Education, Culture, Sports, Science and Technology of Japan. We wish to thank Mr. S. Aizawa and Mr. S. Harada at AKICO Corporation for the design and construction of the experimental apparatus. We also thank Mr. K. Itou for the preparation of the manuscript.

Nomenclature

C_0	=	concentration of a raw material	[mM]
C_i	=	concentration of i-mer of oligoglycine	[mM]

C_i^*	=	concentation of i-mer of oligoglycine compensated by evaporation	[mM]
i	=	degree of condensation	[—]
L	=	rate of the loss of glycine	[—]

Literature Cited

Alargov, D. K., S. Deguchi, K. Tsujii and K. Horikoshi; "Reaction Behaviors of Glycine under Super- and Subcritical Water Conditions," *Origins of Life and Evolution of the Biosphere*, **32**, 1–12 (2002)

Imai, E., H. Honda, K. Hatori, A. Brack and K. Matsuno; "Elongation of Oligopeptides in a Simulated Submarine Hydrothermal System," *Science*, **283**, 831–833 (1999)

Islam, M. N., T. Kaneko and K. Kobayashi; "Reaction of Amino Acids in a Supercritical Water-Flow Reactor Simulating Submarine Hydrothermal Systems," *Bull. Chem. Soc. Jpn.*, **76**, 1171–1178 (2003)

Ogata, Y., E. Imai, H. Honda, K. Hatori and K. Matsuno; "Hydrothermal Circulation of Seawater through Hot Vents and Contribution of Interface Chemistry to Prebiotic Synthesis," *Origins of Life and Evolution of the Biosphere*, **30**, 527–537 (2000)

Pearson, J. D. and M. C. McCroskey; "Perfluorinated Acid Alternatives to Trifluoroacetic Acid for Reversed-Phase High-Performance Liquid Chromatography," *J. Chromatogr., A*, **746**, 277–281 (1996)

Sato, N., H. Daimon and K. Fujie; "Decomposition of Glycine in High Temperature and High Pressure Water," *Kagaku Kogaku Ronbunshu*, **28**, 113–117 (2002)

Shock, E. L.; "Stability of Peptides in High-Temperature Aqueous Solutions," *Geochimi. Cosmochim. Acta*, **56**, 3481–3491 (1992)

Tucker, I. G., M. E. Dowty, M. Veillard, M. A. Longer and J. R. Robinson; "Reversed-Phase High-Performance Liquid Chromatographic Analysis of Oligoglycines (One to Six Amino Acid Residues)," *Pharm. Res.*, **6**, 100–102 (1989)

Journal of Chemical Engineering of Japan, Vol. 39, No. 1, pp. 52–56, 2006

Novel Surface Processing with Sulfonic Acid for Quantum Dot and Its Characteristics

Amane SHIOHARA, Noriyoshi MANABE,
Kazumi OMATA and Kenji YAMAMOTO
Department of Medical Ecology and Informatics, Research Institute, International Medical Center of Japan, 21-1, Toyama 1, Shinjyuku-ku, Tokyo 162-8655, Japan

Keywords: QD-SO_3^-, Surface Processing, Sulfonic Acid, Acidic Conditions

We developed smaller sized quantum dots covered with sodium 2-mercaptoethanesulfonate which has a sulfonyl group (QDs-SO_3^-), and compared its stability in acid, salt and buffer solutions with that of the quantum dots covered with the mercaptoundecanoic acid (QDs-MUA) and covered with the NH_2 group (QDs-NH_2). We found that the QD-SO_3^- well disperses in these solutions without quenching and this stability holds on for 24 h. Next, we investigated the effect of Sheep Serum Albumin (SSA) coating. The SSA coating stabilizes the QD-MUA in the solutions. However, for the QD-SO_3^-, it does not have any significant effect. It implies that the QD-SO_3^- has advantages over the other quantum dots on the stability in the solutions. These results suggest that the novel surface processing using the sulfonyl group expands the possibilities of applications for various fields.

Introduction

The nanometer-size semiconductor is called a quantum dot (QD). The quantum dots are characterized by the following quantum effects: (1) a special photo quality caused by widening the band gap when the spatial dimension is reduced (Unold *et al.*, 2004; Weig *et al.*, 2004); (2) they can produce different colors by changing the sizes (Mattoussi *et al.*, 2000); and (3) they have excellent photostability and their fluorescences can be observed more than 1 h (Hoshino *et al.*, 2004). Because of these interesting characteristics, quantum dots are widely employed for industrial and medical applications. For the industrial applications, they are used as photovoltaics, multicolor LEDs, electronic memory devices, quantum dot barcodes, high throughput chemical and biological sensors (Han *et al.*, 2001; Coe *et al.*, 2002; Santori *et al.*, 2002; Zrenner *et al.*, 2002; Alivisatos., 2004; Clapp *et al.*, 2004). For the medical applications, they are coming into use as immunostaining, a drug delivery system, and so on (Dubertret *et al.*, 2002; Xu *et al.*, 2003; Shiohara *et al.*, 2004). Here, one of the indispensable properties for both applications is their interactions with other materials; especially the interaction with water plays a crucial role for the dispersibility in aqueous solutions. For example, this property is important for integrating quantum dots into devices functionally (Jaffer *et al.*, 2004). A simple way to control the solvation is to modify the surface of the quantum dots. The surface-modified quantum dots synthesized for the first time are covered with non-polar groups of organic molecules such as trioctyl phosphine oxide (TOPO), so that they are insoluble in water, putting some limitations on their functions in aqueous conditions. This problem was solved by Chan and Nie (1998). They synthesized water-soluble quantum dots, CdSe/QD-MUA, the surface of which are covered with mercaptoundecanoic acid (MUA). This QD-MUA was made by the method of substituting non-polar groups of organic molecules on the surface of quantum dots for MUA. The QD-MUA made a tremendous contribution to the possibility of application of quantum dots for various fields not only industry but also medical biology (Huang *et al.*, 1998; Åkerman *et al.*, 2002; Hanaki *et al.*, 2003; Gao *et al.*, 2004; Hoshino *et al.*, 2004; Wu and Bruchez, 2004; Santra *et al.*, 2005).

A further important problem is that the QD-MUA is not stable in acid or it coheres easily in buffer solution. This should be an impediment to medical 3 applications, and it might also cause a problem in the field of industry. Hanaki *et al.* (2003) have succeeded to stabilize QD-MUA under physiological conditions by coating it with sheep serum albumin (SSA), and the purpose of the present work is to develop their study. We investigated CdSe/QD covered with sodium 2-mercaptoethanesulfonate (QD-SO_3^-) and focused on its compatibility with various solvents. The reasons we chose this ligand are as follows. First, the sulfonyl group is a strong acid, and secondly this ligand can be

Received on May 18, 2005. Correspondence concerning this article should be addressed to K. Yamamoto (E-mail address: backen@ri.imcj.go.jp).

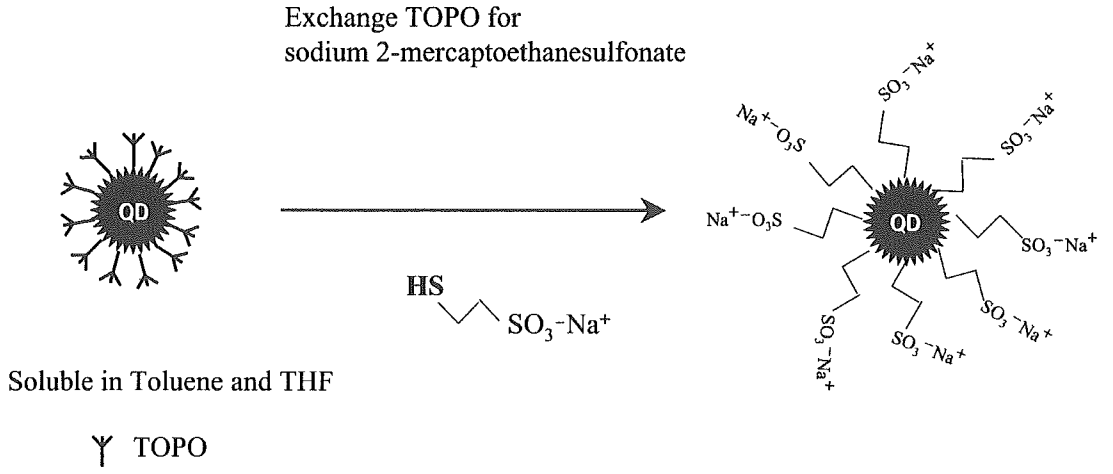

Fig. 1 Synthesis of QD-SO_3^-

connected with an alkyl chain followed by the terminal group, SH. In this study, (1) we succeeded in synthesis of QD-SO_3^- for the first time; (2) we compared the stability of QD-SO_3^- with that of quantum dots with NH_2 connected to two alkyl groups (QD-NH_2) and QD-MUA in acid and buffer solutions; and (3) we studied those quantum dots coated with SSA to conduct the experiments under conditions similar to Hanaki *et al.* (2003).

1. Materials and Methods

1.1 Preparation of QD-MUA, QD-NH_2 and QD-SO_3^-

The quantum dots with the core of CdSe and the shell of ZnS (see **Figure 1**) were synthesized from the QD-tri-*n*-octylphosphine oxide (QD-TOPO). After QD-TOPO (Murray *et al.*, 1993; Hines and Guyot-Sionnest, 1996; Peng *et al.*, 1997) dissolved in tetrahydrofuran (Wako Pure Chemical Industries, Ltd.), the solution was warmed up to 85°C, and sodium 2-mercaptoethanesulfonate (Shionogi & Co., Ltd.), MUA (Sigma-Aldrich Co.) and cysteamine hydrochloride (Wako Pure Chemical Industries, Ltd.) dissolved in ethanol were dripped into it. It was reflexed for 12 h. Then, for the sodium 2-mercaptoethanesulfonate and MUA, 100 μL of the NaOH solution (pH 10) was added into them to ionize the quantum dots, and the tetrahydrofuran was evaporated at 90°C. The unrefined quantum dots thus obtained, were refined and concentrated with an ultrafiltration membrane (Microcon YM-3, Millipore Corp.) and sephadex column (MicroSpin G-25 Columns, Amersham Bioscience Corp.), and then each of the refined quantum dot was obtained. To coat the quantum dots with SSA, we mixed the solutions of quantum dots and SSA.

1.2 Preparation of acid, buffer and salt solutions

The acidic conditions were provided by sulfuric acid. The observation range was 0.25 mM (pH 3.2)–0.001 mM (pH 5.1). The pH of borate buffer solution was pH 9. The concentration of the salt solutions were 1 M NaCl and 5 M NaCl. The PBS and MEM were used as salt solutions as well. The concentration of QD-MUA, QD-NH_2, and QD-SO_3^- was 0.1 mg/mL. As for these quantum dots, the powder of each quantum dot was weighed and 10 mg/mL aqueous solution was made. Then the solutions were diluted into 0.1 mg/mL. The quantum dots were added to each solution and they were observed 1 h and 24 h after.

Table 1 Particle size and surface potential of each quantum dot

	Particle size [nm]	Zeta potential [mV]
QD-SO_3	10.12	−32.74
QD-MUA	19.97	−32.31
QD-NH_2	10.36	10.95

The particle size and surface potential of each quantum dot was measured with Zetasizer (Malvern Instruments Ltd.) after filtration. A 0.45 μm filter was used for this experiment.

2. Result

2.1 Spectrum intensity, size distribution, and zeta potential

We measured the fluorescent intensity of QD-MUA, QD-NH_2, and QD-SO_3^-. The spectra are shown in **Figure 2**. The fluorescent peak intensity of QD-MUA was about 3 times as large as that of QD-SO_3^-. However, that of QD-NH_2 was 3 times lower than that of QD-SO_3^-.

The results of the particle sizes and the zeta potential are shown in **Table 1**. The particle diameter of QD-SO_3^- is 10.12 ± 3.247 nm. On the other hand, 80% of the provided QD-MUA have the particle diameter

Table 2 Stability of each quantum dot for acid, salts, base, and buffer

	QD-SO_3		QD-SO_3-SSA		QD-MUA		QD-MUA-SSA		QD-NH_2	
	1 h	o/n	1 h	o/n	1 h	o/n	1 h	o/n	1 h	o/n
Water	+	+	+	+	+	+	+	+	+	–
0.25 mM H_2SO_4/pH 3.2	+	–	+	+	q	q	+	–	q	q
0.1 mM H_2SO_4/pH 3.7	+	+	+	+	q	q	+	+	+	–
0.01 mM H_2SO_4/pH 4.6	+	+	+	+	+	+	+	+	+	–
Borate buffer/pH 9	+	+	+	+	+	–	+	+	+	+
1 M NaCl	+	+	+	+	–	–	+	–	–	–
5 M NaCl	+	+	+	+	–	–	+	–	q	q
PBS	+	+	+	+	–	–	+	–	–	–
MEM	+	+	+	+	–	–	+	+	+	–

+: dispersion, –: aggregation, q: quenching
Stabilities of each quantum dot for acid, salts, base, and buffer solutions were measured with 0.1 mg/mL of concentration of each quantum dot. And photos were taken after 1 h and overnight. o/n shows after overnight.

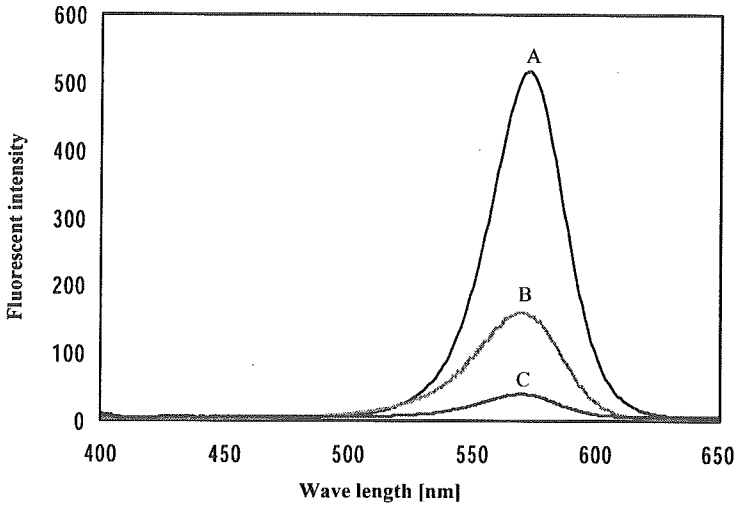

Fig. 2 Emission spectra of each quantum dot. Spectra A stands for QD-MUA, spectra B and spectra C stand for QD-SO_3^- and QD-NH_2 respectively. Each quantum dot was dissolved in distilled water and their emission spectra were measured with FP-6500. Each quantum dot was excited at 350 nm. Concentration of each quantum dot was 0.1 mg/mL

of 19.97 ± 6.563 nm. The diameter of the rest is 572 ± 418 nm but these particles probably aggregated in water. The diameter of QD-NH_2 is 10.36 ± 3.224 nm, which is almost the same size as that of QD-SO_3^-. The zeta potentials of QD-SO_3^-, QD-MUA and QD-NH_2 were –32.7, –32.3, and +10.95 mV, respectively. The results of these measurements were consistent with what we can predict from the structure of each quantum dot.

2.2 Stability in acid, salts, base, and buffer solution

The results about the stability of the quantum dots are summarized in **Table 2**. Here, the stability stands for the condition that quantum dots disperse and give off light in the solutions in this study. In acid, salt, and buffer solutions, the non-coat QD-SO_3^- is stable except the case of pH 3.2 after 24-h incubation. The SSA-coated QD-SO_3^- is always stable in all the solutions. The stability of the non-coated QD-MUA was quite low and quenching was occurred in acid (see **Figure 3**). The SSA-coated QD-MUA was stable under all the acidic conditions after 1-h incubation and in NaCl solutions as well in this experiment, but it aggregates at pH 3.2 and NaCl solutions after 24 h. The QD-NH_2 generally was not stable in all the solutions after 24 h.

3. Discussion

Our study is based on the prediction that QD-SO_3^- shows high stability in low pH solutions because this surface ligand is expected to be compatible with the sulfuric acid. Thus, let us compare the stability of QD-SO_3^-, QD-MUA and QD-NH_2 in detail.

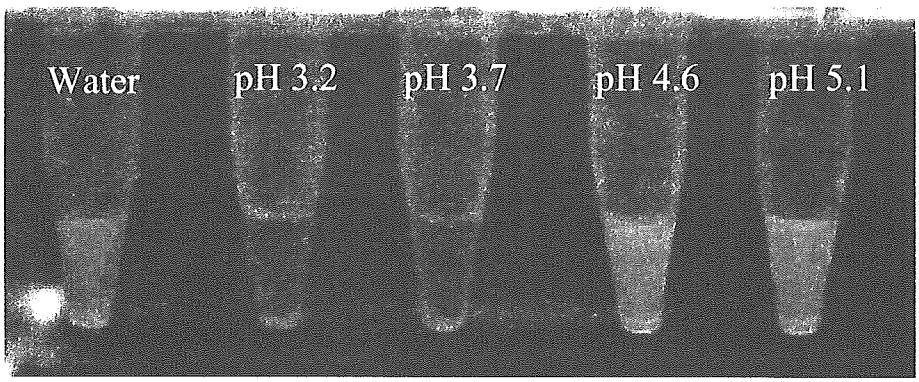

Fig. 3 Representative results of QD-MUA. Photos were taken after 24 h. The pictures stand for QD-MUA in water, acidic solutions of pH 3.2, 3.7, 4.6 and 5.1 from the left-hand side, respectively

Firstly, we compare the stability of the quantum dots without the SSA coating. Under acidic conditions, the QD-SO_3^- is more stable than the QD-MUA (see the second and third rows in Table 2). The QD-MUA undergoes quenching under the acidic conditions, pH 3.2 and pH 3.7. There are several possibilities for the reasons of the quenching: (1) the surface states of the quantum dots are changed by the acidic solvent; (2) the exciting energy is transformed to energy other than fluorescence; and (3) the ZnS shell of the quantum dot is destroyed by the acidic solvent. Among them, the last possibility is the most plausible because the quenching occurred rapidly when the quantum dots was added into the solvent. This quenching results from the fact that the sulfonyl group of QD-SO_3^- is more compatible with the sulfuric acid than the carboxyl group of the QD-MUA and the ZnS shell of the QD-SO_3^- can be protected. In addition, the hydrophobic alkyl group in the ligand of QD-MUA is longer than that of QD-SO_3^- so that the ligands might prevent each other from bonding to the surface of the quantum dot during the synthesis process. As a result, the number of surface ligands of the QD-MUA is smaller than that of the QD-SO_3^-, and the ZnS shell is easily attacked by the acidic molecules.

Also in the buffer and salt solutions, the non-coated QD-SO_3^- is more stable than the non-coated QD-MUA (see the fifth to ninth rows in Table 2). This is because the ionization of the sulfonyl group of the QD-SO_3^- is larger than the carboxyl group of the QD-MUA. Accordingly, the surface of QD-SO_3^- is not easily terminated by hydrogen and the polarity of the QD-SO_3^- can be kept in the buffer and salt solutions.

Secondly, we compare the SSA-coated and non-coated quantum dots and discuss the effect of the SSA coating. While Hanaki *et al.* (2003) have already reported that SSA raises the dispersibility of QD-MUA in MEM (see the last row in Table 2), we found that the same effect can be observed for the SSA-coated QD-MUA in acid and borate buffer as well. This result indicates that the SSA coating the surface of the quantum dots prevents the contact of the quantum dots each other, regardless of the kind of solvents. On the contrary, it is noteworthy that there is no remarkable difference between the SSA-coated QD-SO_3^- and no-coated QD-SO_3^-. For the QD-SO_3^-, SSA coating has no significant effect for the stability in acid, buffer, and salt solutions. This result implies that the QD-SO_3^- has a great advantage over the QD-MUA as for dispersion in solutions.

For industrial applications, SSA coating is not always needed because additional processes of the surface coating take one's time and the SSA must be denatured at high temperature. Concerning this point, the QD-SO_3^- coated with SSA has an important meaning for biological applications. The SSA coating has significant roles of carrying the quantum dots into cells, and without coating, they do not get inside cells (data not shown).

Finally, we mention an advantageous property of the QD-SO_3^-. The QD-SO_3^- has smaller particle size than the QD-MUA: the diameter of the QD-SO_3^- is about a half compared to QD-MUA. This means that the QD-SO_3^- is more suitable for the use in immunostaining.

It is desirable for industrial applications to determine the threshold of the stability against acids. For this purpose, the titration is a better way to give their exact values. We are about to perform such experiments in the future work.

Acknowledgment

We thank Dr. Richard Tilley at Victoria University in Wellington and Hideki Maruyama at Shionogi & Co., Ltd. for the important discussion and help. We were supported by Grants-in-Aid for the Advancement of Medical Equipment of the Ministry of Health, Labor and Welfare and Japan Association.

Literature Cited

Åkerman, M. E., W. C. W. Chan, P. Laakkonen, S. N. Bhatia and E. Ruoslahti; "Nanocrystal Targeting *in vivo*," *Proc. Natl. Acad. Sci. U.S.A.*, **99**, 12617–12621 (2002)

Alivisatos, P.; "The Use of Nanocrystals in Biological Detection," *Nat. Biotechnol.*, **22**, 47–52 (2004)

Chan, W. C. W. and S. Nie; "Quantum Dot Bioconjugates for Ultrasensitive Nonisotopic Detection," *Science*, **281**, 2016–2018 (1998)

Clapp, A. R., I. L. Medintz, J. M. Mauro, B. R. Fisher, M. G. Bawendi and H. Mattoussi; "Fluorescence Resonance Energy Transfer between Quantum Dot Donors and Dye-Labeled Protein Acceptors," *J. Am. Chem. Soc.*, **126**, 301–310 (2004)

Coe, S., W.-K. Woo, M. Bawendi and V. Bulović; "Electroluminescence from Single Monolayers of Nanocrystals in Molecular Organic Devices," *Nature*, **420**, 800–802 (2002)

Dubertret, B., P. Skourides, D. J. Norris, V. Noireaux, A. H. Brivanlou and A. Libchaber; "*In vivo* Imaging of Quantum Dots Encapsulated in Phospholipid Micelles," *Science*, **298**, 1759–1762 (2002)

Gao, X., Y. Cui, R. M. Levenson, L. W. K. Chung and S. Nie; "*In vivo* Cancer Targeting and Imaging with Semiconductor Quantum Dots," *Nat. Biotechnol.*, **22**, 969–976 (2004)

Han, M., X. Gao, J. Z. Su and S. Nie; "Quantum-Dot-Tagged Microbeads for Multiplexed Optical Coding of Biomolecules," *Nat. Biotechnol.*, **19**, 631–635 (2001)

Hanaki, K., A. Momo, T. Oku, A. Komoto, S. Maenosono, Y. Yamaguchi and K. Yamamoto; "Semiconductor Quantum Dot/Albumin Complex Is a Long-Life and Highly Photostable Endosome Marker," *Biochem. Bioph. Res. Co.*, **302**, 496–501 (2003)

Hines, M. A. and P. Guyot-Sionnest; "Synthesis and Characterization of Strongly Luminescing ZnS-Capped CdSe Nanocrystals," *J. Phys. Chem.*, **100**, 468–471 (1996)

Hoshino, A., K. Hanaki, K. Suzuki and K. Yamamoto; "Applications of T-Lymphoma Labeled with Fluorescent Quantum Dots to Cell Tracing Markers in Mouse Body," *Biochem. Bioph. Res. Co.*, **314**, 46–53 (2004)

Huang, P., P. L. Olive and R. E. Durand; "Use of the Comet Assay for Assessment of Drug Resistance and Its Modulation *in vivo*," *British, Journal of Cancer*, **77**, 412–416 (1998)

Jaffar, S., K. T. Nam, A. Khademhosseini, J. Xing, R. S. Langer and A. M. Belcher; "Layer-by-Layer Surface Modification and Patterned Electrostatic Deposition of Quantum Dots," *Nano Lett.*, **4**, 1421–1425 (2004)

Li, X., Y. Wu, D. Steel, D. Gammon, T. H. Stievater, D. S. Katzer, D. Park, C. Piermarocchi and L. J. Sham; "An All-Optical Quantum Gate in a Semiconductor Quantum Dot," *Science*, **301**, 809–811 (2003)

Mattoussi, H., J. M. Mauro, E. R. Goldman, G. P. Anderson, V. C. Sundar, F. V. Mikulec and M. G. Bawendi; "Self-Assembly of CdSe-ZnS Quantum Dot Bioconjugates Using an Engineered Recombinant Protein," *J. Am. Chem. Soc.*, **122**, 12142–12150 (2000)

Murray, C. B., D. J. Norris and M. G. Bawendi; "Synthesis and Characterization of Nearly Monodisperse CdE (E = Sulffur, Selenium, Tellunium) Semiconductor Nanocrystallites," *J. Am. Chem. Soc.*, **115**, 8706–8715 (1993)

Peng, X., M. C. Schlamp, A. V. Kadavanich and A. P. Alivisatos; "Epitaxial Growth of Highly Luminescent CdSe/CdS Core/Shell Nanocrystals with Photostability and Electronic Accessibility," *J. Am. Chem. Soc.*, **119**, 7019–7029 (1997)

Santori, C., D. Fattal, J. Vučković, G. S. Solomon and Y. Yamamoto; "Indistinguishable Photons from a Single-Photon Device," *Nature*, **419**, 594–597 (2002)

Santra, S., H. Yang, P. H. Holloway, J. T. Stanley and R. A. Mericle; "Synthesis of Water-Dispersible Fluorescent, Radio-Opaque, and Paramagnetic CdS:Mn/ZnS Quantum Dots: A Multifunctional Probe for Bioimaging," *J. Am. Chem. Soc.*, **127**, 1656–1657 (2005)

Shiohara, A., A. Hoshino, K. Hanaki, K. Suzuki and K. Yamamoto; "On the Cyto-Toxity Caused by Quantum Dots," *Microbiol. Immunol.*, **48**, 669–675 (2004)

Unold, T., K. Mueller, C. Lienau, T. Elsaesser and A. D. Wieck; "Optical Stark Effect in a Quantum Dot: Ultrafast Control of Single Exciton Polarizations," *Phys. Rev. Lett.*, **92**, 157401 (2004)

Weig, E. M., R. H. Blick, T. Brandes, J. Kirschbaum, W. Wegscheider and M. Bichler and J. P. Kotthanus; "Single-Electron-Phonon Interaction in a Suspended Quantum Dot Phonon Cavity," *Phys. Rev. Lett.*, **92**, 046804 (2004)

Wu, X. and M. P. Bruchez; "Labeling Cellular Targets with Semiconductor Quantum Dot Conjugates," Methods Cell Biology, vol. 75, Cytometry, 4th ed., pp. 171–183, Academic Press, New York, U.S.A. (2004)

Xu, H., M. Y. Sha, E. Y. Wong, J. Uphoff, Y. Xu, J. A. Treadway, A. Truong, E. O'Brien, S. Asquith, M. Stubbins, N. K. Spurr, E. H. Lai and W. Mahoney; "Multiplexed SNP Genotyping Using the Qbead System: A Quantum Dot-Encoded Microsphere-Based Assay," *Nucleic Acids Res.*, **31**, e43 (2003)

Zrenner, A., E. Beham, S. Stufler, F. Findeis, M. Bichler and G. Abstreiter; "Coherent Properties of a Two-Level System Based on a Quantum-Dot Photodiode," *Nature*, **418**, 612–614 (2002)

Am J Physiol Endocrinol Metab 289: E419–E428, 2005.
First published April 12, 2005; doi:10.1152/ajpendo.00512.2004.

Proteomic analysis on insulin signaling in human hematopoietic cells: identification of CLIC1 and SRp20 as novel downstream effectors of insulin

Kumiko Saeki,[1,*] Etsuko Yasugi,[1,*] Emiko Okuma,[1] Samuel N. Breit,[4] Megumi Nakamura,[3] Tosifusa Toda,[3] Yasushi Kaburagi,[2] and Akira Yuo[1]

[1]*Departments of Hematology and* [2]*Metabolic Disorder, Research Institute, International Medical Center of Japan;* [3]*Proteomics Collaboration Research Group, Tokyo Metropolitan Institute of Gerontology, Tokyo, Japan;* and [4]*Centre for Immunology, St. Vincent's Hospital, and University of New South Wales, Sydney, Australia*

Submitted 27 October 2004; accepted in final form 11 April 2005

Saeki, Kumiko, Etsuko Yasugi, Emiko Okuma, Samuel N. Breit, Megumi Nakamura, Tosifusa Toda, Yasushi Kaburagi, and Akira Yuo. Proteomic analysis on insulin signaling in human hematopoietic cells: identification of CLIC1 and SRp20 as novel downstream effectors of insulin. *Am J Physiol Endocrinol Metab* 289: E419–E428, 2005. First published April 12, 2005; doi:10.1152/ajpendo.00512.2004.—Insulin/IGF-I-dependent signals play important roles for the regulation of proliferation, differentiation, metabolism, and autophagy in various cells, including hematopoietic cells. Although the early protein kinase activation cascade has been intensively studied, the whole picture of intracellular signaling events has not yet been clarified. To identify novel downstream effectors of insulin-dependent signals in relatively early phases, we performed high-resolution two-dimensional electrophoresis (2-DE)-based proteomic analysis using human hematopoietic cells 1 h after insulin stimulation. We identified SRp20, a splicing factor, and CLIC1, an intracellular chloride ion channel, as novel downstream effectors besides previously reported effectors of Rho-guanine nucleotide dissociation inhibitor 2 and glutathione *S*-transferase-pi. Reduction in SRp20 was confirmed by one-dimensional Western blotting. Moreover, MG-132, a proteasome inhibitor, prevented this reduction. By contrast, upregulation of CLIC1 was not observed in one-dimensional Western blotting, unlike the 2-DE results. As hydrophilic proteins were predominantly recovered in 2-DE, the discrepancy between the 1-DE and 2-DE results may indicate a certain qualitative change of the protein. Indeed, the nuclear localization pattern of CLIC1 was remarkably changed by insulin stimulation. Thus insulin induces the proteasome-dependent degradation of SRp20 as well as the subnuclear relocalization of CLIC1.

HL-60 cells; PDQuest; matrix-assisted laser desorption ionization coupled to time-of-flight mass spectrometry; Mascot

INSULIN AND INSULIN-LIKE GROWTH FACTOR I (IGF-I) are known as important regulators of a variety of biological effects, including growth, development, and metabolism. Moreover, insulin-dependent signals contribute to the regulation of azurophil granule-selective macroautophagy in human hematopoietic cells (16). The molecular mechanisms for the actions of insulin and IGF-I have been intensively studied by various approaches, including gene-targeting animal experiments (1, 8, 14, 22) and molecular cloning techniques (20, 21). Now, the scenario for early intracellular signal transduction including a protein kinase activation cascade is well documented. It has been revealed that common intracellular signaling pathways are working downstream of insulin and IGF-I, including insulin receptor substrates (IRSs) (12) and Shc (17). The IRSs phosphorylate phosphatidylinositol 3-kinase to activate Akt, which transmits signals for proliferation and survival as well as the hematopoietic macroautophagy regulation (16), and the mammalian target of rapamycin and S6 kinase, which transmit signals for growth and translation besides heaptic macroautophagy regulation (2). On the other hand, Shc transmits signals for differentiation in hematopoietic cells (25).

In contrast to the early signal transduction, the picture of the later signaling events remains rather obscure. A large number of still undetermined molecules may be working downstream of the insulin-dependent signals. To obtain the whole picture of the intracellular signaling events downstream of the insulin receptor, comprehensive studies such as transcriptome analysis and proteome analysis may be especially powerful. A transcriptome analysis can illuminate the intracellular signaling events if they require new transcriptions or altered message stabilities. However, changes in protein expression are not always associated with those of the message expression, and vice versa. Thus transcriptome analysis would occasionally bring about false positive and/or false negative results. In this sense, proteome analysis is thought to be a more practical tool. Moreover, proteome analysis has merit in demonstrating protein modification changes such as phosphorylation and acetylation besides the change in net expression amounts. Indeed, studies on proteome analysis have successfully identified the protein molecules associated with metabolic regulation in the liver (3, 7). However, proteome analysis on insulin signaling in hematopoietic cells has not been performed despite the significance of insulin-dependent signals in the hematopoietic system.

For the first time, we performed proteomic analysis using human hematopoietic cells with the high-resolution two-dimensional electrophoresis (2-DE) system. We show that SRp20, a splicing factor, and CLIC1, an intracellular chloride ion channel, are working as novel downstream effectors of insulin signaling. The biological relevance of these events is discussed.

MATERIALS AND METHODS

Cells, growth factors, and inhibitors. HL-60 cells were maintained in RPMI 1640 medium (Life Technologies, Grand Island, NY) supplemented with 10% heat-inactivated fetal calf serum (FCS; JRH Bioscience, Lenexa, KS). For insulin-stimulating experiments, cells

* These authors contributed equally to this work. The order of the authors' names was arbitrarily arranged.

Address for reprint requests and other correspondence: A. Yuo, Dept. of Hematology, Research Institute, International Medical Center of Japan, 1-21-1 Toyama, Shinjuku-ku, Tokyo 162-8655, Japan (e-mail: yuoakira@ri.imcj.go.jp).

The costs of publication of this article were defrayed in part by the payment of page charges. The article must therefore be hereby marked "*advertisement*" in accordance with 18 U.S.C. Section 1734 solely to indicate this fact.

had been previously cultured in serum-free RPMI 1640 medium supplemented with 5 μg/ml human holo-transferrin (Sigma Chemical, St. Louis, MO) for 3 days, and then 5 μg/ml insulin (Sigma) were added. Transferrin was suspended in RPMI 1640 medium, and insulin was solubilized by 1 N hydrochloride. In some experiments, MG-132 (Calbiochem, La Jolla, CA) was added 30 min before insulin stimulation.

Two-dimensional gel electrophoresis with quantitative analyses. Insulin-depleted cells were stimulated by insulin. After a 1-h incubation, stimulated and nonstimulated cells were collected. After a washing with wash buffer (10 mM Tris·HCl buffer, pH 8.0, 5 mM magnesium acetate), 4×10^7 cells were suspended with 7 volumes of lysis buffer containing 2 M thiourea, 7 M urea, 4% (wt/vol) CHAPS, and 1 mM Pefabloc SC PLUS (Roche Diagnostics, Mannheim, Germany). The cell suspensions were kept for 10 min on ice, sonicated intermittently, and centrifuged at 12,000 *g* for 10 min at 4°C, and the supernatant fractions were collected. The protein concentration was determined in the lysis solution with a dye reagent from Amersham Biosciences (Piscataway, NJ), using BSA as a standard. The lysate was alkylated with Ready Prep Reduction-Alkylation Kit (Bio-Rad Laboratories, Hercules, CA). The 120 μg of protein lysate per gel were subjected to two-dimensional gel electrophoresis (2-DE). One-dimensional isoelectric focusing was carried out using Immobiline dry strip (18 cm long, pH 3–10 nonlinear or pH 4–7 linear, Amersham Biosciences) in a horizontal electrophoresis system (Ettan IPGphor, Amersham Biosciences) according to the manufacturer's instructions. After the one-dimensional elecrofocusing, IPG gels were equilibrated with buffer containing 50 mM Tris·HCl (pH 8.8), 6 M urea, 30% (vol/vol) glycerol, 2% (wt/vol) sodium dodecyl sulfate (SDS), 0.01% bromophenol blue, and 0.5% dithiothreitol, followed by alkylation with equilibration buffer containing 4.5% idoacetamide instead of 0.5% dithiothreitol at room temperature for 15 min. The gels were subjected to two-dimensional SDS-PAGE (10% gel). Proteins were visualized in the gels by staining with SYPRO Ruby Protein Gel Stain (Bio-Rad Laboratories) for overnight. The florescence intensity of each protein spot was digitally recorded by FluorImager 595 (Amersham Biosciences) using ImageQuaNT software and the differential protein expression quantitatively analyzed by PDQuest software (Bio-Rad Laboratories). The density of each spot was normalized by that of the smallest β-actin spot. Initially, all of the spots were roughly matched by an automatic program in PDQuest software, which was followed by a more detailed manual matching process to correct inappropriate matching pairs. Three to six independent experiments were performed, and the results were statistically analyzed by Student's *t*-test.

Mass spectrometric analysis. Mass spectrometric analysis was performed according to the method reported by Toda et al. (23), with slight modifications. Briefly, each protein spot in SYPRO Ruby-stained gels was picked by FluoroPhoreStar 3000 (Anatech, Tokyo, Japan). The pieces of gels were dehydrated in 50% acetonitrile and 50% ammonium bicarbonate, next in 100% acetonitrile, and dried. The proteins were digested with 5 μg/ml trypsin (sequencing grade modified trypsin; Promega, Madison, WI) at 30°C. After overnight protein digestion, peptide fragments in the digest were subjected to matrix-assisted laser desorption ionization (MALDI) coupled to a time-of-flight (TOF) (MALDI-TOF) mass spectrometer (AXIMA-CFR; Shimazdu, Kyoto, Japan) for peptide mass fingerprinting (PMF). Protein identification was performed with the Mascot server (Matrix Science, Boston, MA) and Protein Prospector (UCSF Mass Spectrometry Facility, San Francisco, CA). We selected the *Homo sapiens* database of SWISS-PROT and parameters: peptide tolerance ± 0.4 Da and one missed cleavage. Carbamidomethyl modification of cysteine and acetylation of the NH_2-terminal end or lysine and phosphorylation of serine, threonine, or tyrosine were considered. Protein identification was repeated at least once with spots from different gels. Phosphorylated peptides were confirmed by MALDI-TOF-MS in a postsource decay (PSD) mode of AXIMA-CFR and AXIMA-CFRplus (Shimadzu). NH_2-terminal acetylation was determined by MALDI-QIT-TOF-MS in an MS/MS mode (AXIMA-QIT, Shimadzu).

One-dimensional Western blotting. Cells (5×10^5) were lysed with 100 μl of 1× Laemmli's sample buffer and boiled. Ten microliters of this lysate were subjected to SDS-PAGE with 15% gels. The electric transfer onto a polyvinylidene difluoride (PVDF) membrane was carried out with a semidry blotting apparatus (Bio-Rad Laboratories) at 50 mA/cm^2 for 45 min at room temperature using buffer containing 2.25% Tris, 10.8% glycine, and 20% methanol. The first antibody reaction was performed using anti-SRp20 antibody (7B4; Santa Cruz Biotechnology, Santa Cruz, CA), anti-Rho-guanine nucleotide dissociation inhibitor (Rho-GDI) antibody (A-20; Santa Cruz Biotechnology), anti-β-tubulin antibody (H-235; Santa Cruz Biotechnology), a sheep anti-CLIC1 antiserum (25), anti-cyclin D3 antibody (C-16; Santa Cruz Biotechnology), anti-cyclin E antibody (M-20; Santa Cruz Biotechnology), and anti-cyclin A antibody (BF683; Upstate Biotechnology, Lake Placid, NY). The second antibody reaction and the final detection procedure were performed using ECL Western blotting detection reagents (Amersham Biosciences) or SuperSignal West Dura Extended Duration Substrate (Pierce Biotechnology, Rockford, IL) according to the manufacturers' guidance. Information of the chemical luminescence was analogically developed onto Hyperfilm (Amersham Biosciences). After scanning of the developed film, the band intensities were calculated by ImageQuant software (Amersham Biosciences). Stripping of the first antibody was performed by incubating the PVDF membrane with Restore Western Blot Stripping Buffer (Pierce Biotechnology) at room temperature for 30 min.

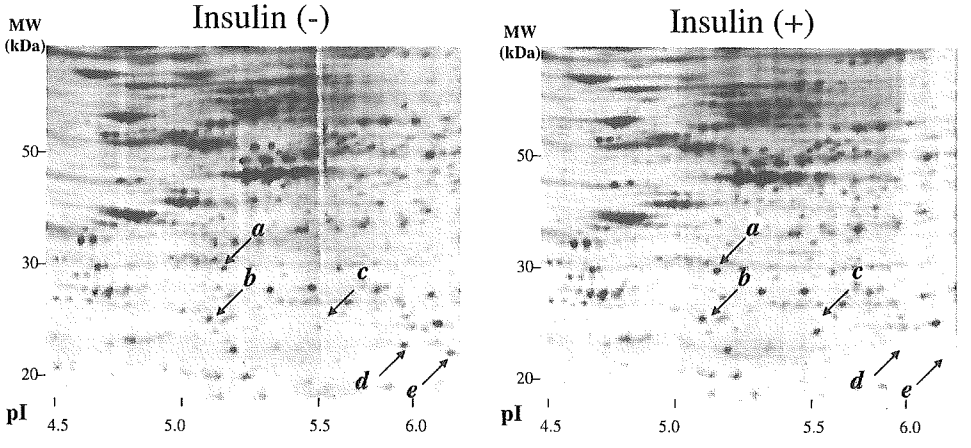

Fig. 1. Two-dimensional electrophoresis (2-DE) profile of human hematopoietic HL-60 cells with or without insulin treatment. HL-60 cells were cultured with transferrin-supplemented serum-free medium for 3 days. Then buffer solution (*left*) or 5 μg/ml insulin (*right*) was added, and cells were cultured for another 1 h at 37°C. Cell lysates were prepared as described in Experimental Procedures, and 2-DE was carried out. PDQuest software-based analysis demonstrated that the 5 spots (indicated by arrows) showed significant differences in their expressions with or without insulin treatment. *Spot a,* CLIC1, an intracellular chloride ion channel; *spot b,* Rho-guanine nucleotide dissociation inhibitor 2 (Rho-GDI-1); *spot c,* and glutathione *S*-transferase-pi (GST-pi); *spots d* and *e,* SRp-20, a splicing factor; *isoform of β-actin.

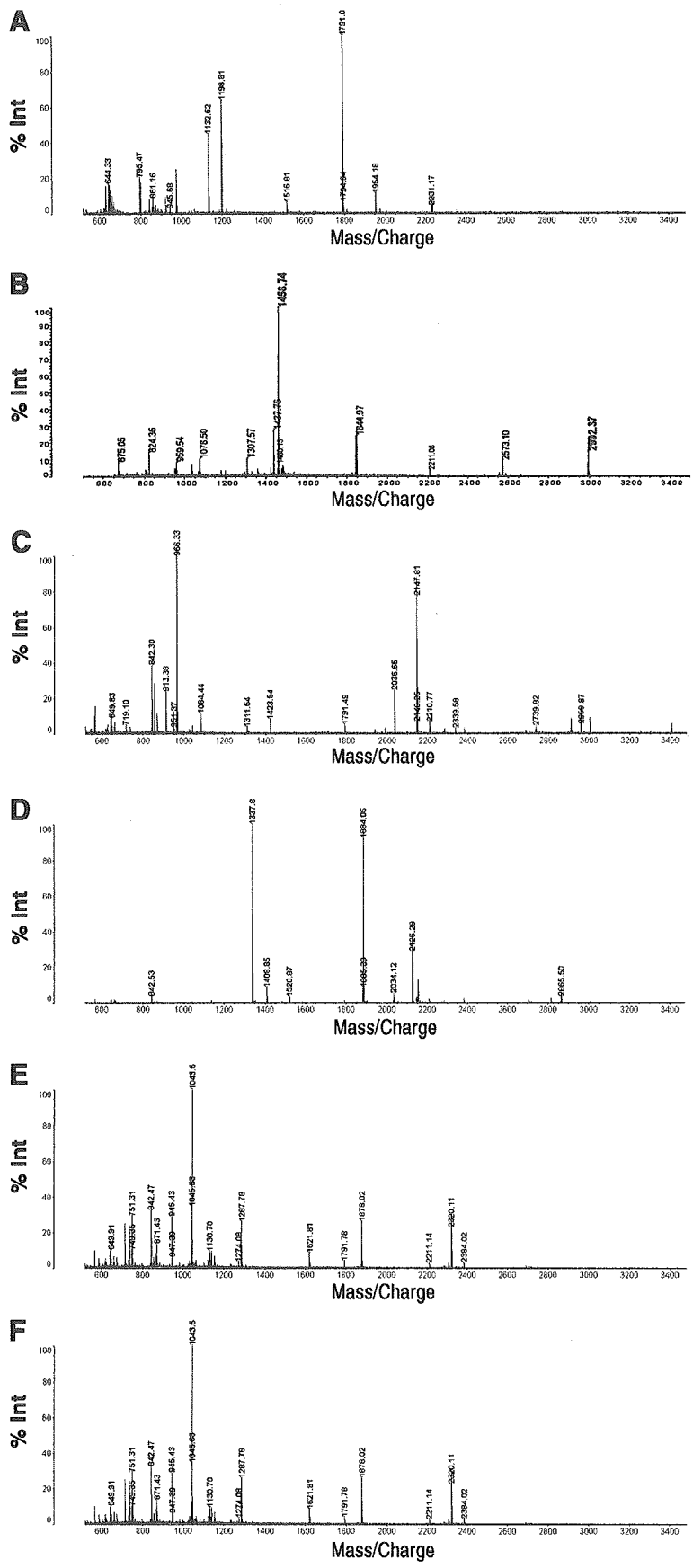

Fig. 2. Peptide mass fingerprinting (PMF) of *spots a–e*. *Spots a* (*B*), *b* (*C*), *c* (*D*), *d* (*E*), *e* (*F*) were picked, and, after trypsin digestion, matrix-assisted laser desorption ionization coupled to a time-of-flight mass spectrometer (MALDI-TOF-MS) analysis was performed. As a positive control, a β-actin spot (* in Fig. 1) was picked and analyzed (*A*).

Two-dimensional Western blotting. SYPRO Ruby-stained proteins on gels were resolubilized and transferred according to our previously reported method (23). Briefly, the stained gel was incubated in resolubilization buffer (0.2% wt/vol SDS, 0.3% wt/vol Tris, 0.7% wt/vol glycine) for 10 min and mounted onto a PVDF membrane in a semidry blotting apparatus (Bio-Rad Laboratories). Electrotransfer was carried out at 4 V/cm^2 for 1 h at room temperature using buffer containing 0.3% (wt/vol) Tris, 1.5% (wt/vol) glycine, 0.1% (wt/vol) SDS. The florescence images of the blotted PVDF membranes were scanned and recorded by FluorImager 595 (Amersham Biosciences). The PVDF membranes were further subjected to immunoblotting as in cases of 1-DE Western blotting.

Cell cycle analysis. Cells (5×10^5) were collected, washed with PBS, and fixed with 70% ice-cold ethanol for 4 h. After treatment with RNase A (100 μg/ml, Sigma) for 30 min at 37°C, DNA was stained with 50 μg/ml propidium iodide (Sigma). Cell cycle analysis was performed by FACScalibur (Becton-Dickinson, Mountain View, CA) using CELL Quest software according to the manufacturer's guidance.

Immunocytochemistry. Cells were fixed on slide glasses with a cytospin apparatus (Cytospin2; Shandon, Pittsburgh, PA) with further fixation with acetone-methanol solution (1:3). The immunostaining procedure was performed as described elsewhere (16) using anti-CLIC1 antibody (1:1,000 dilution) (24). The cells were observed by fluorescent microscopy with Normarsky differentiated interference contrast (Olympus Optical, Tokyo, Japan).

Statistical analysis. Student's *t*-test was used to determine statistical significance. A P value of <0.05 was considered significant.

RESULTS

2-DE protein expression profiles of human hematopoietic cells with or without insulin treatment. To identify novel downstream effectors in early phases of insulin-dependent signals in human hematopoietic cells, we performed the 2-DE-based differential protein expression analysis using human myeloblastic HL-60 cells. The cells which had been cultured in the absence of insulin for 3 days were treated with 5 μg/ml insulin or water. After 1 h, cell lysates were prepared according to the standard isoelectric focusing electrophoresis method described in MATERIALS AND METHODS. In this procedure, highly hydrophobic, urea-insoluble proteins were eliminated during the centrifugation step as precipitants, and only the supernatant fractions were used for 2-DE. In preliminary experiments, we used the immobilized pH gradient gel strip with a broad pH range (pH 3–10 nonlinear) for one-dimensional isoelectric focusing. Although more than 1,000 protein spots were visualized after SYPRO Ruby staining, PDQuest software-based analysis indicated that the spots having significant expression changes by insulin treatment were mainly located at pH 4–6 in the horizontal axis (data not shown). Thus we performed the following detailed analysis using the immobilized pH gradient gel strip with a narrower range (pH 4–7 linear) for finer resolution (Fig. 1). Over 600 protein spots were visualized by SYPRO Ruby staining. From these spots, we selected the candidates for the subsequent mass spectrometric analysis according to the following criteria. The basal expression level was higher than 5% of that of the largest β-actin spot, and the increase or decrease in the expression after insulin stimulation was greater than twofold or less than one-half, respectively. After statistical analysis of the multiple experiments (n = 3–6), five candidates were determined (Fig. 1). These spots were picked from the gel and, after trypsin digestions, MALDI-TOF-MS analysis was performed. Figure 2 shows the PMF of each spot, with a PMF of β-actin as a positive control. These data were further analyzed, being sent to the Mascot search server, and it was suggested that *spot a* was CLIC1, *spot b* was Rho-GDI-2, *spot c* was glutathione *S*-transferase-pi (GST-pi), and *spots d* and *e* were SRp20 (Fig. 2 and Table 1). The Mascot score of each search result was 175 (*spot a*), 80 (*spot b*), 98 (*spot c*), 100 (*spot d*), and 64 (*spot e*), indicating that the protein identifications by PMF were highly reliable (the data are summarized in Table 1). The results of the statistical analysis for the expression amounts of these spots are summarized in Table 2. Among these spots, Rho-GDI-2 (*spot b*) and GST-pi (*spot c*) have already been identified as downstream effectors of insulin. Rho-GDI-2 is reportedly released from the intracellular membrane fractions to the cytoplasm by insulin (19), and the expression of GST-pi markedly increases after insulin stimulation (6). Thus we focused our research on the evaluation of *spot a* and *spots d* and *e*.

To confirm the Mascot search results, we performed 2-DE western blotting by transferring SYPRO Ruby-stained 2-DE protein spots to PVDF membrane. As shown in Fig. 3*A*, most of the proteins were properly transferred to the membrane with a SYPRO Ruby pattern similar to that of the original gel. As shown in Fig. 3*B*, *spot a* was indeed recognized by anti-CLIC1

Table 2. *Ratios of spot intensities (insulin+/insulin−)*

Spot	Protein	Means ± SD	P Value
a	CLIC1	1.83±0.37	<0.01
b	Rho-GDI-2	2.03±0.43	<0.02
c	GST-pi	1.93±0.52	<0.05
d	SRp20	0.24±0.33	<0.01
e	SRp20	0.18±0.27	<0.005

Summarized results from 3–6 independent experiments are shown. Statistical analysis was performed by Student's *t*-test.

Table 1. *Protein identification by mass spectrometry analysis*

Spot	GenBank Acc. No.	Protein Name	Mr		pI		Mascot Score	Peptides		Sequence Coverage, %
			Theo, Da	O bs, kDa	Theo	Obs		Match	Total	
a	O00299	CLIC1	2,7248	29.0	5.09	5.16	175	10	11	47
b	P52566	Rho-GDI-2	2,3031	23.6	5.10	5.08	80	6	9	24
c	P09211	GST-pi	2,3438	22.9	5.44	5.67	98	6	8	48
d	P23152	SRp20	1,9546	21.2	11.64	6.13	100	9	11	43
e	P23152	SRp20	1,9546	20.5	11.64	6.38	100	9	11	43

Values of theoretical isoelectric points (pI) and molecular weights/masses (Mr) were obtained from Mascot search results. Theo, theoretical; Obs, observed; CLIC1, intracellular chloride ion channel; Rho-GDI-2, Rho-guanine nucleotide dissociation inhibitor 2; GST-pi, glutathione-*S*-transferase-pi; SRp20, a splicing factor. Calculations of experimental isoelectric point (pI) and molecular weight (Mr) were based on migration of the protein spot on 2-D gels using PDQuest.

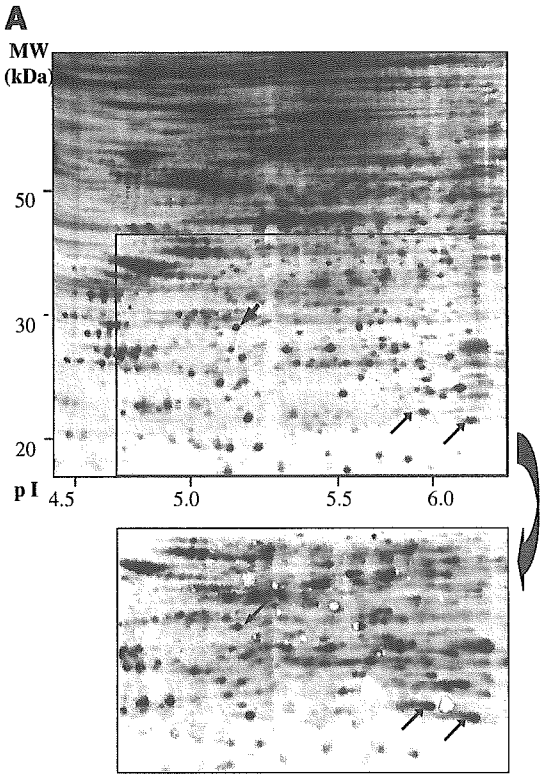

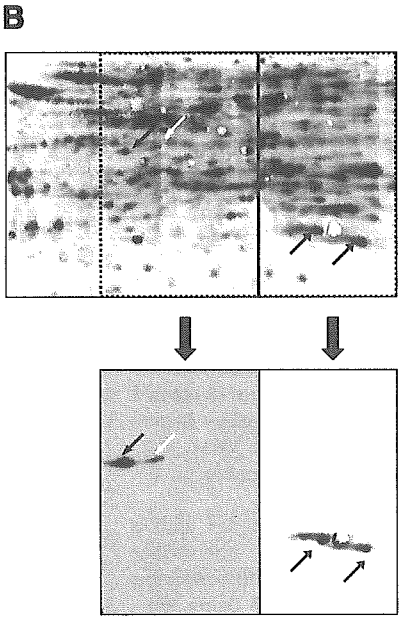

Fig. 3. 2-DE Western blotting. *A*: SYPRO Ruby-stained 2-DE gel, in which the lysate of buffer solution-treated cells were applied as in Fig. 1, *left*, was trimmed (*top*) and transferred onto a PVDF membrane (*bottom*). Transferred proteins were visualized by fluorescence image scanner. *B*: PVDF membrane was cut as indicated and blotted by anti-CLIC1 antiserum (*bottom left*) or anti-SRp20 antiserum (*bottom right*). Spots for CLIC1 and SRp20 are indicated with black arrows. Note that there is an extra spot on the anti-CLIC1-blotted membrane (indicated with white arrow).

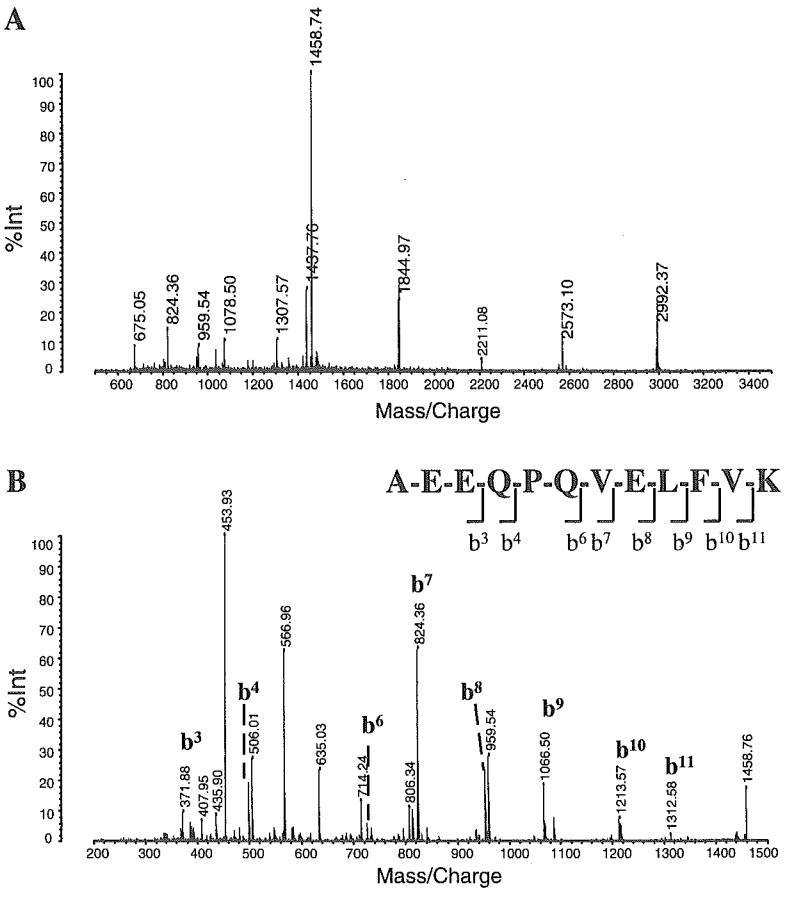

Fig. 4. Amino acid sequencing of NH_2-terminal peptide fragment of CLIC1. Parent ion at *m/z* 1,458.74 in Fig. 2*B* in insulin-treated cells was subjected to subsequent analysis using MS/MS mode of MALDI-TOF-MS (AXIMA-QIT). The mass data of b-series of the product ions were analyzed by the PepSeq program in ProteinLynx software. NH_2-terminal acetylated peptides of *N*-acetyl-AEE (*m/z* 372.14, b^3 ion), *N*-acetyl-AEEQ (*m/z* 500.20, b^4 ion), *N*-acetyl-AEEQPQ (*m/z* 725.30, b^6 ion), *N*-acetyl-AEEQPQV (*m/z* 824.38, b^7 ion), *N*-acetyl-AEEQPQVE (*m/z* 953.42, b^8 ion), *N*-acetyl-AEEQPQVEL (*m/z* 1,066.50, b^9 ion), *N*-acetyl-AEEQPQVELF (*m/z* 1,213.57, b^{10} ion), and *N*-acetyl-AEEQPQVELFV (*m/z* 1,312.64, b^{11} ion) were detected. Peptide mass fingerprinting (PMF; *A*) and MS/MS data of b-series (*B*) are shown. Similar analysis concerning control cells also demonstrated NH_2-terminal acetylation of CLIC1 (data not shown).

antibody and *spots d* and *e* were recognized by anti-SRp20 antibody. We also studied the possible modifications on these two proteins. As shown in Fig. 1*A*, the observed isoelectric point (pI) of CLIC1 was 5.16, which is similar to the Mascot information (the calculated pI was 5.09). Interestingly, there was an extra small spot with a higher pI value (Fig. 3*B*, white arrow). Indeed, we detected a doublet band in one-dimensional Western blotting, where the lysate prepared for 2-DE was mixed with an isovolume of 2× Laemmli's sample buffer and subjected to SDS-PAGE (data not shown and see Fig. 6*B*). Thus CLIC1 is expressed in at least two forms with different pI values in human hematopoietic cells, although the molecular basis for this difference was not elucidated. The MS digest analysis of *spot a* in the 2-DE profiles of both the insulin-treated and control cells demonstrated that the peptide fragment at mass-to-charge ratio (*m/z*) 1,458.74 in PMF of *spot a* represented the NH_2 terminus acetylated fragment acetyl-AEEQPQVELFVK, indicating that the first methionine was eliminated and the second alanine was N-acetylated. This finding was indeed confirmed by the amino acid sequencing at the *m/z* 1,458.74 fragment by the MS/MS mode of MALDI-TOF-MS, as shown in Fig. 4.

As for SRp20, the observed pI values of *spots d* and *e* were 6.13 and 6.38, respectively (Fig. 1 and Table 1), in contrast to the Mascot software information (the calculated pI was 11.64). This discrepancy may come from the modifications of SRp20. The MS digest analysis indicated that the SRp20 was phosphorylated at two sites, including Ser^{115} and Ser^{108}, from the existence of the peptide fragment ions of *m/z* 751.31 and *m/z* 945.43 (Fig. 5*A*). Mass value of *m/z* 751.31 is speculated amino acid sequences as $RRSPR_{(113-117)}$, $RSPRR_{(114-118)}$, or $SPRRR_{(115-119)}$ (Fig. 5*E*). As concerns *m/z* 945.43, MS digest suggests the amino acid sequence as $RRSPPPR_{(106-112)}$, $RSPPPRR_{(107-113)}$, or $SPPPRRR_{(108-114)}$. Phosphorylated peptide was confirmed by MALDI-TOF-MS in a seamless PSD mode (AXIMA-CFR) that detected the neutral loss of phosphate group. As shown in Fig. 5, *B* and *C*, phosphorylation-dependent neutral loss (−80 Da) and dehydration (−18 Da) were detected in the fragments at *m/z* 751.31 and *m/z* 945.43. Conversely, the MALDI-TOF-MS PSD spectrum of the control peptide ion gated at *m/z* 1,043.57 showed no significant neutral loss (Fig. 5*D*). Next, the amino acid sequences of *m/z* 751.31, *m/z* 945.43, and *m/z* 1,043.57 were examined by the same method as described above by using AXIMA-CFRplus. The amino acid sequences of *m/z* 751.31 could not be determined because the fragment ion was low intensity (data not shown). However, it is presumable that the Ser^{115} is phosphorylated. From the mass spectra of gated ion at *m/z* 945.43, the amino acid sequence was determined as $RRSPPPR_{(106-112)}$, and the position of phosphorylation was Ser^{108} (Fig. 6*A*). As a

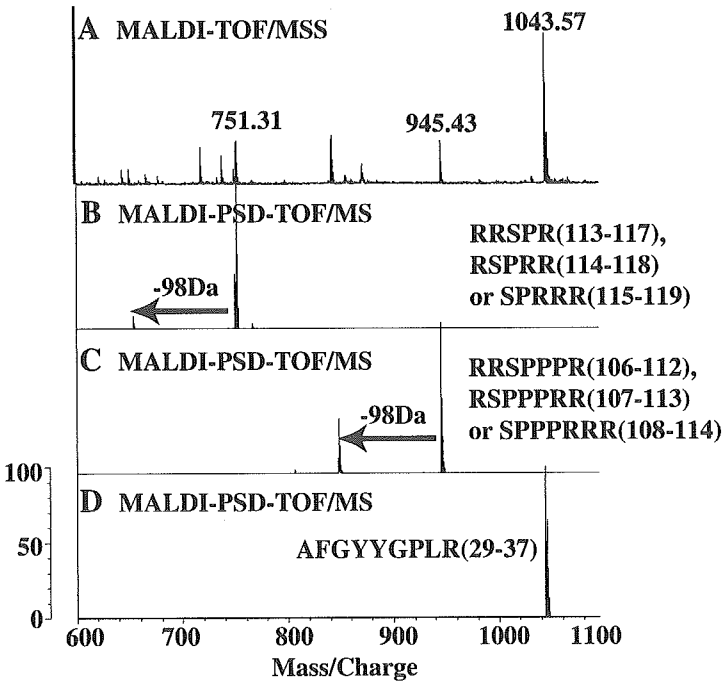

Fig. 5. Confirmation of SRp20 phosphorylation at specific serine residues. *A*: gated ions at *m/z* 751.31, 945.43, and 1,043.57 in Fig. 2*E* were subjected to analysis of neutral loss by MALDI-TOF-MS (AXIMA-CFR) in post-source decay (PSD) mode. The 98-Da loss of mass values was detected in gated ion at *m/z* 751.31 (*B*) and *m/z* 945.43 (*C*), but not in gated ion at *m/z* 1,043.57 (*D*) as a negative control. *E*: primary sequence of SRp20. *Phosphorylated amino acid.

E 1 MHRDSCPLDC KVYVGNLGNN GNKTELERAF GYYGPLRSVW VARNPPGFAF

m/z 1043.57

51 VEFEDPRDAA DAVRELDGRT LCGCRVRVEL SNGEKRSRNR GPPPSWGRRP

101 RDDYRRR*PP PRRR*PRRRS FSRSRSRSLS RDRRRERSLS RERNHKPSRS

m/z 945.43 *m/z* 751.31

151 FSRSRSRSRS NERK

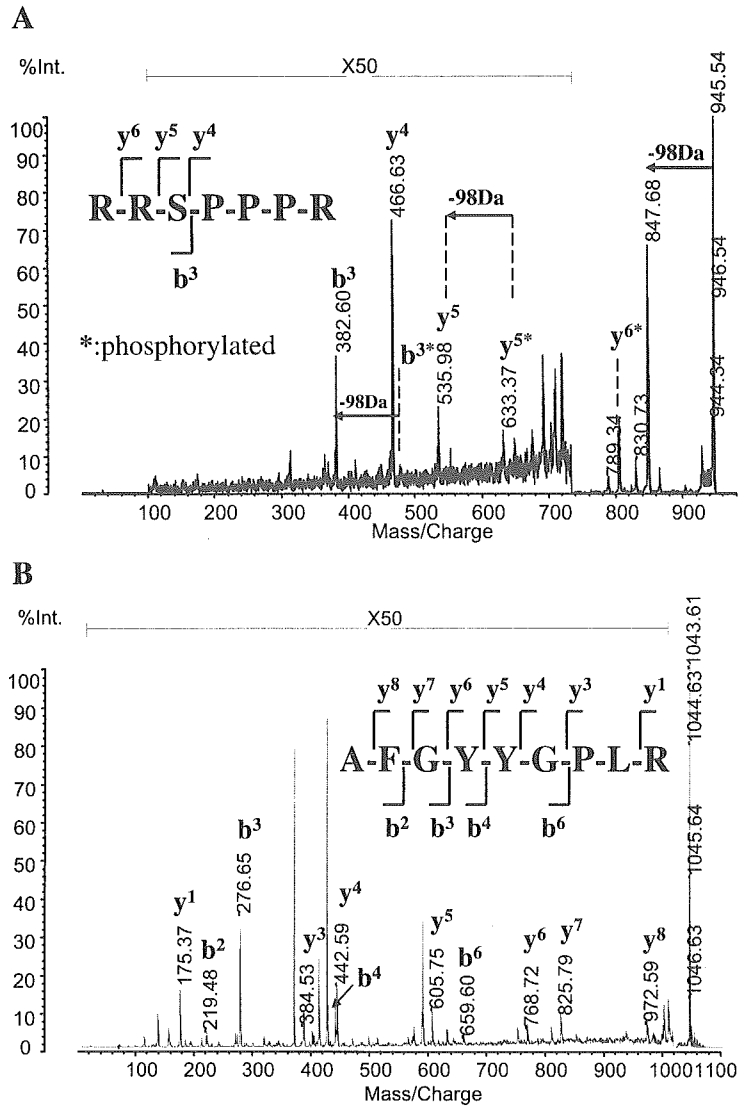

Fig. 6. Sequence analysis of gated ions at *m/z* 945.43 and 1,043.57 by MALDI-TOF-MS in PSD mode. *A*: gated ion at *m/z* 945.29 in Fig. 5*C* was subjected to subsequent analysis using PSD mode of MALDI-TOF-MS (AXIMA-CFRplus) *B*: three neutral loss ions (−98 Da) of *m/z* 480, 633, and 945 were detected. Gated ion at *m/z* 1,043.57 in Fig. 5*D* was subjected to the same analysis. Neutral loss ion (−98 Da) was not detected.

negative control, *m/z* 1,043.57 was subjected to analysis using PSD mode of AXIMA-CFRplus (Fig. 6*B*). The amino acid sequence was decided as AFGYYGPLR$_{(29-37)}$, which was not phosphorylated. These results indicated that Ser^{115} and Ser^{108} were phosphorylated in human hematopoietic cells (Fig. 5*E*). Thus the two phosphorylations of SRp20 may be responsible for the acidic shift of SRp20 in 2-DE.

Thus the 2-DE-based differential protein expression analysis identified CLIC1 and SRp20 as novel downstream effectors of insulin in human myeloblastic HL-60 cells.

1-DE study of CLIC1 and SRp20 expressions after insulin stimulations. It is known that there are occasionally discrepancies between the results of 2-DE and 1-DE. The difference in the protein solubilization capacities between the two systems is thought to be one of the reasons. During cell lysate preparation in 2-DE, highly hydrophobic proteins are prone to make precipitations and thus be eliminated from the lysates after centrifugation. Thus the protein expression changes in 2-DE-based proteome analysis not only means that the net protein expression changes but also the changes in protein solubilization. So we studied the expressions of CLIC1 and SRp20 after insulin stimulation by 1-DE Western blotting.

In contrast to the results of 2-DE, there was no significant difference in CLIC1 expression between insulin-treated and nontreated samples in 1-DE (Fig. 7*A*). Moreover, CLIC1 was detected as a single band, unlike the 2-DE results, where CLIC1 was detected as two spots. Interestingly, CLIC1 was detected as a doublet band, and the expression amounts of CLIC1 were indeed upregulated by insulin stimulation when the 2-DE lysates were treated by an isovolume of 2× Laemmli's buffer and subjected to 1-DE (Fig. 7*B, lane 2*). These findings strongly suggest that insulin treatment induced certain qualitative changes of CLICL1. Compared with 1-DE, the protein recovery rate in 2-DE was generally low: one-fourth the recovery as for CLIC1 (Fig. 7*B*, compare *lanes 1* and *3*) and one-eighth the recovery as for β-tubulin (Fig. 7*B*, compare *lanes 1* and *3*). However, the expression amounts of β-tubulin (Fig. 7*B*, compare *lanes 1* and *2*) and α-tubulin (data not shown) were not significantly changed by insulin treatment even in 2-DE lysates. By contrast, around a twofold increment in CLIC1 was reproducibly observed after insulin stimulation (Fig. 7, *B* and *C*, and data not shown). We then examined the possibility that the insulin-mediated increments in CLIC1 in 2-DE lysate were associated with the changes in its subcellular

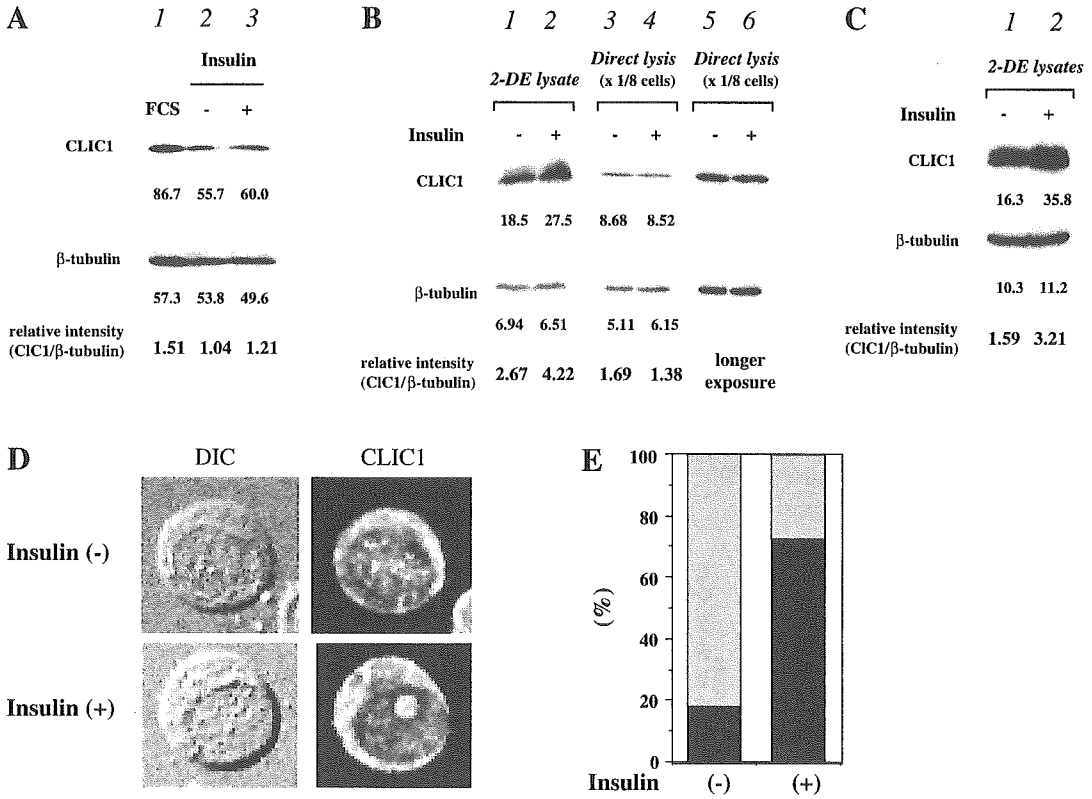

Fig. 7. 1-DE Western blotting of CLIC1. Cells that had been cultured with transferrin-supplemented serum-free medium for 3 days were stimulated by buffer solution (*lane 2*) or insulin (*lane 3*) and incubated for another 1 h at 37°C. *A*: cells were directly lysed with 1× Laemmli's sample buffer and subjected to 1-DE. Western blotting was performed using anti-CLIC1 antiserum. The lysate of the cells that had been cultured in the presence of FCS was also subjected to 1-DE (*lane 1*). Numeral under each band indicates intensity of the protein band. After the first antibody was stripped, the PVDF membrane was reblotted with anti-β-tubulin antibody. *B*: cell lysates prepared according to 2-DE protocol were mixed with isovolume of 2× Laemmli's sample buffer (*lanes 1* and *2*). One-eighth of the cells were directly lysed with 1× Laemmli's sample buffer and subjected to 1-DE (*lanes 3* and *4*). Longer exposure results of *lanes 3* and *4* are shown in *lanes 5* and *6*, respectively. *C*: results of independently performed experiment from *B* are shown. *D* and *E*: subcellular localization of CLIC1. *D*: insulin-treated or nontreated HL-60 cells were stained with anti-CLIC1 antibody. DIC, photograph with Normarsky differentiated interference contrast. *E*: percentages of cells with nuclear speckled staining pattern (filled bars) and cells with nucleoli-staining pattern (gray bars) are shown.

localization. As shown in Fig. 7, *D* and *E*, the nuclear localization pattern of CLIC1 was clearly changed by insulin treatment: CLIC1 was detected mainly as speckled forms in nuclear matrix in nontreated cells, whereas CLIC1 was located mainly at nucleoli in insulin-treated cells. Thus the changes in subnuclear localization may responsible for the expressional changes of CLIC1 in 2-DE.

Next, we studied the expression of SRp20 in 1-DE Western blotting. The SRp20 expression was actually reduced as in the case of 2-DE (Fig. 8*A*), indicating that the total amount of SRp20 was reduced by insulin treatment. To further investigate the molecular basis of insulin-mediated reduction in SRp20, the effects of the proteasome inhibitor MG-132 were examined. As shown in Fig. 8*B*, MG-132 inhibited the insulin-mediated reduction of SRp20 in a dose-dependent manner. MG-132 also blocked the degradation of cyclin D3 and enhanced the accumulation of cyclin D3 after insulin stimulation (Fig. 8*B*, *lane 5*). Interestingly, the recovery of SRp20 expres-

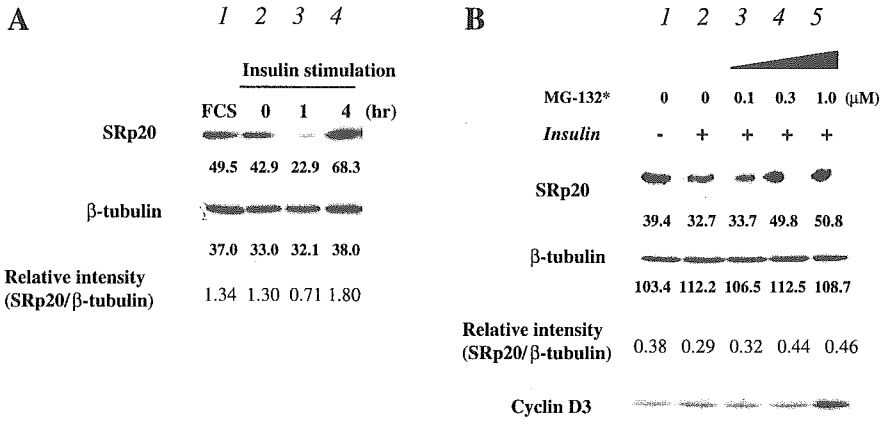

Fig. 8. 1-DE Western blotting of SRp20. Cells were cultured with transferrin-supplemented serum-free medium for 3 days. *A*: cells were then stimulated with insulin, and cell lysates were prepared at indicated times (*lanes 2–4*). Western blotting was performed using anti-SRp20 antiserum. The lysate of cells cultured in the presence of FCS was also subjected to 1-DE (*lane 1*). Numeral under each band indicates intensity of protein band. After the first antibody was stripped, PVDF membrane was reblotted with anti-β-tubulin antibody. *B*: DMSO or increasing doses of MG-132 were added 30 min before insulin stimulation. Cell lysates were prepared 1 h after stimulation and subjected to 1-DE. Western blotting was performed using anti-SRp20 antiserum. PVDF membrane was reblotted with anti-β-tubulin antibody and further with cyclin D3 antibody.